High-Field Transport in n-Type GaAs

E. M. CONWELL AND M. O. VASSELL
The Bayside Laboratory, Research Center of General Telephone & Electronic Laboratories, Bayside, New York

(Received 29 August 1967)

We have solved the coupled Boltzmann equations for the electron distributions in Γ_1 and X_1 minima of GaAs under a set of approximations that are fair for fields around the beginning of the negative-differential-resistance region, but should be quite good at higher fields. Intervalley, polar and other relevant intravalley scattering processes have been included. Nonparabolicity of the central minimum has been taken into account. The effect of space-charge scattering has also been considered. From the distributions, we have calculated as functions of field the average drift velocity, the variation of the valley populations, diffusion constants, and mobilities in each of the valleys, etc. The validity of the principal approximations made, such as neglect of the L_1 minima, is discussed. The present experimental situation is examined, and some tentative explantations are offered for the large differences between the various measurements of drift velocity versus field.

1. INTRODUCTION

THE discovery of the Gunn effect[1] has stimulated great interest in the high-field transport of n-type GaAs. A sizable number of investigations, both theoretical and experimental, have been carried out. It is the purpose of the present paper to describe in detail our calculations of the distribution functions and, from these, the drift velocity and other transport properties as a function of field. Preliminary accounts of some aspects of this work have been published elsewhere.[2–6] We shall also compare our results with other theoretical results and with experimental results insofar as is possible.

We begin with a summary, comprising Secs. 2–4, of what is known about band structure and transport in GaAs and of the model we have used in our calculations. In Sec. 5 the Boltzmann equation for the central valley, with nonparabolicity included, is set up for the energy range in which transitions to the upper valleys are not possible and its solution obtained. The Boltzmann equation for the upper valleys is then set up in Sec. 6 and the coupled equations solved. From the distributions are calculated drift velocity, valley populations, mobilities, diffusion constants and average energies of the carriers in Sec. 7, and some comparisons with experiment are carried out. In the final section the validity of the principal approximations made, both in the model and in the calculations, is discussed. Comparisons are made with other theoretical calculations, and the present experimental situation is discussed.

2. BAND STRUCTURE OF GaAs

Information about the band structure of GaAs has been obtained from many experiments and, recently, from theoretical calculations by the pseudopotential[7] and $\mathbf{k}\cdot\mathbf{p}$[8] methods. Experiment[9] and theory agree that the conduction-band minimum is at the center of the Brillouin zone, spherically symmetric at not too high energies and nonparabolic. With the approximation that the band gap ε_G is much larger than the spin-orbit splitting energy, the dependence of energy ε on wave vector $\mathbf{k}$ in the central minimum may be written[9]

$$\varepsilon(\mathbf{k})=(\hbar^2k^2/2m_0)+(\varepsilon_G/2)[(1+4\varepsilon_p\hbar^2k^2/2m_0\varepsilon_G^2)^{1/2}-1], \tag{2.1}$$

where m_0 is the free-electron mass and ε_p is $2/m_0$ times the square of the momentum matrix element connecting the conduction, light mass, and splitoff valence bands. For later purposes it is useful to rewrite (2.1) in the form

$$(\hbar^2k^2)/2m_0 = \varepsilon+(\varepsilon_G+\varepsilon_p)[1-\{1+4\varepsilon\varepsilon_p/(\varepsilon_G+\varepsilon_p)^2\}^{1/2}]/2. \tag{2.2}$$

For small ε the radical may be expanded, giving

$$\frac{\hbar^2k^2}{2m_0}=\varepsilon\left[\frac{\varepsilon_G}{\varepsilon_G+\varepsilon_p}+\frac{\varepsilon_p^2\varepsilon}{(\varepsilon_G+\varepsilon_p)^3}-\frac{2\varepsilon_p^3\varepsilon^2}{(\varepsilon_G+\varepsilon_p)^5}\cdots\right]. \tag{2.3}$$

In the limit $\varepsilon\to 0$, the right-hand side of (2.3) must approach $\varepsilon m_1/m_0$, where m_1 is the mass at the bottom of the band. Taking this mass as 0.072 m_0, and $\varepsilon_G=1.5$ eV, Ehrenreich deduced that $\varepsilon_p=20$ eV.[9] Using the fact that $\varepsilon_G/(\varepsilon_G+\varepsilon_p)=m_1/m_0$, we may write, finally,

$$(\hbar^2k^2/2m_1)\equiv\gamma(\varepsilon)=\varepsilon[1+\alpha\varepsilon+\beta\varepsilon^2+\cdots], \tag{2.4}$$

[1] J. B. Gunn, IBM J. Res. Develop. 8, 141 (1964).
[2] E. M. Conwell and M. O. Vassell, Trans. IEEE ED-13, 22 (1966).
[3] M. O. Vassell and E. M. Conwell, Phys. Letters 21, 612 (1966).
[4] E. M. Conwell, Phys. Letters 21, 368 (1966).
[5] E. M. Conwell and M. O. Vassell, Appl. Phys. Letters 9, 411 (1966).
[6] E. M. Conwell and M. O. Vassell, in *Proceedings of the International Conference on the Physics of Semiconductors, Kyoto, 1966* [J. Phys. Soc. Japan Suppl. 21, 527 (1966)].
[7] M. L. Cohen and T. K. Bergstresser, Phys. Rev. 141, 789 (1966). This paper will be referred to as BC.
[8] F. H. Pollak, C. W. Higginbotham, and M. Cardona, in *Proceedings of the International Conference on the Physics of Semiconductors, Kyoto, 1966* [J. Phys. Soc. Japan Suppl. 21, 20 (1966)]. This paper will be referred to as PHC. We are indebted to Professor Cardona for a copy of this paper (unpublished).
[9] H. Ehrenreich, Phys. Rev. 120, 1951 (1960).

where $\alpha=\varepsilon_p^2/\varepsilon_G(\varepsilon_G+\varepsilon_p)^2$, $\beta=-2\varepsilon_p^3/\varepsilon_G(\varepsilon_G+\varepsilon_p)$.[4] For GaAs, $\alpha=0.576/\text{eV}$ and $\beta=-0.050/(\text{eV})^2$. It is seen that the contribution of terms in β and beyond in the series (2.4) may be neglected even at energies as high as 1 eV. It must be noted also that the accuracy of the relations (2.1) through (2.4) should begin to diminish at $\varepsilon\sim 1$ eV because they neglect the effect of higher minima.

It was established by Ehrenreich[9] from a consideration of several different kinds of data—variation of resistivity with pressure, Hall effect at high temperatures, and the behavior of the band gap in Ga(As,P) alloys—that the next higher minima are along the ⟨100⟩ directions, 0.36 eV above the (0,0,0) minimum. These experiments do not, unfortunately, give the location of the minima along ⟨100⟩. According to the theoretical calculations[7,8] these minima appear to be at the edge of the Brillouin zone and to have X_1 symmetry. The next minima above the ⟨100⟩ ones were expected to be along the ⟨111⟩ directions,[9] and Hilsum[10] suggested, from experimental evidence, that they are 0.5 eV above the bottom of the conduction band. From further consideration of their photoemission data,[11] Eden and Spicer[12] have concluded it is likely that these minima are within 0.2 eV of the X_1 minima. At 0.5 eV above the band edge they would be only about $5k_0T$ at room temperature above the X_1 minima. If they were perceptibly closer than this it should not have been possible to make a clearcut distinction between ⟨100⟩ and ⟨111⟩, as was done by Ehrenreich.[9] Thus it seems reasonable that the ⟨111⟩ minima are no lower than, say, 0.45 eV above the band edge. This order of the minima, it is to be noted, is in contradiction to the theoretical calculations, which place the ⟨111⟩ minima, which have L_1 symmetry, either a tenth of a volt below[7] or at about the same energy[8] as the ⟨100⟩ minima. The theoretically calculated energies are not expected to be reliable to more than a few tenths of an electron volt, but this certainly provides additional evidence that the L_1 minima are very close in energy to X_1.

The calculations show another set of minima at the zone edge along the ⟨100⟩ directions, not too far from the X_1 minima. These higher minima have X_3 symmetry. According to the PHC[8] calculation the X_1-X_3 distance is about 1 eV, while in the BC[7] calculation it is only a few tenths of an eV. Since in any case the density of states appears to be much smaller in X_3 than in X_1, neglect of this set of minima is justified.

For both X_1 and L_1 minima the constant energy surfaces in the neighborhood of the band edge are ellipsoidal. PHC have calculated the transverse mass m_t for the X_1 minima to be $0.23m_0$. They could not, unfortunately, obtain the longitudinal mass m_l for these minima. For the ⟨100⟩ minima in silicon, $m_t=0.19m_0$ and $m_l=0.98m_0$, while for those of GaP the calculations of PHC give $m_t=0.28m_0$, $m_l=1.5m_0$. Thus m_t of GaAs is intermediate between m_t of Si and GaP, and, expecting that m_l is similarly placed, one might guess that $m_l\simeq 1.3m_0$. This would give a geometric mean mass $\bar{m}=0.41m_0$, and a density of states mass $m^{(N)}$ of $0.85m_0$ for 3 minima. With the m_l and m_t values of PHC for the L_1 minima we obtain a geometric mean mass of $0.24m_0$ and a density-of-states mass $0.59m_0$. For the present calculations, $m^{(N)}$ for the ⟨100⟩ minima in GaAs was taken to be $1.2m_0$, the value estimated by Ehrenreich[9] from high-temperature Hall data. This would appear to be high for the case of 3 minima, and could, of course, mean that m_l and m_t are larger than estimated above. However, if the ⟨111⟩ minima are as low as 0.5 eV, which is only about $2k_0T$ at the temperatures for which the Hall data were taken, it is to be expected that they also would have been populated and have contributed to the density-of-states mass attributed to the ⟨100⟩ minima. The total density-of-states mass for X_1 and L_1, according to the numbers above, is $1.4m_0$. The ⟨111⟩ minima were neglected in the calculations that follow. If the masses of PHC are correct, however, the use of $m^{(N)}=1.2m_0$ should go a long way toward compensating for this neglect.

3. TRANSPORT IN THE CENTRAL VALLEY

Low-field transport, i.e., transport of carriers in the ⟨0,0,0⟩ valley, has been studied extensively for GaAs. Ehrenreich has shown that, of the possible scattering processes, polar optical scattering predominates at room temperature and low fields.[9] To determine which processes are important at high fields it would be useful to compare the relaxation times and rates of energy loss for the different processes. For the polar optical scattering a relaxation time exists only for carrier energies large compared to $\hbar\omega_l$, the longitudinal optical phonon energy. This relaxation time for the simple model of the band structure with band edge at energy ε_0 is given by[13]

$$(1/\tau_{po})=eE_0(2N_{ql}+1)/[2m(\varepsilon-\varepsilon_0)]^{1/2}, \quad (3.1a)$$

while for a nonparabolic band with spherical symmetry and $\varepsilon_0=0$ it is shown in the Appendix to be

$$(1/\tau_{po})=eE_0(2N_{ql}+1)(d\gamma/d\varepsilon)/(2m_1\gamma)^{1/2}. \quad (3.1b)$$

In these expressions e is the charge on the electron, N_{ql} the number of longitudinal optical phonons, γ the quantity defined by Eq. (2.4), m_1 the mass at the band edge, and E_0 an effective electric field that determines the strength of the electron coupling to the polar modes. Specifically,

$$eE_0\equiv\frac{me^2}{\hbar^2}\hbar\omega_l\left(\frac{1}{\kappa_\infty}-\frac{1}{\kappa_0}\right)=\frac{4\pi me^2e^{*2}}{M\hbar\omega_l v_a}, \quad (3.2)$$

[10] C. Hilsum, in *Physics of Semiconductors* (Academic Press Inc., New York, 1964), p. 1127.

[11] R. C. Eden, J. L. Moll, and W. E. Spicer, Phys. Rev. Letters **18**, 597 (1967).

[12] R. C. Eden and W. Spicer, Stanford University (private communication).

[13] D. J. Howarth and E. H. Sondheimer, Proc. Roy. Soc. (London) **A219**, 53 (1953). See also the Appendix of this paper.

where κ_0 and κ_∞ are the dielectric constants for 0 and ∞ frequencies, respectively, e^* is the effective ionic charge, M the reduced mass of the two ions in the unit cell, and v_a the volume of the cell. With the constants in Ehrenreich's paper,[9] which are listed in Table I, one obtains $E_0=5.95\times10^3$ V/cm, corresponding to $e^*=0.186e$. In more recent measurements values differing by as much as 10% have been obtained for the various constants,[10] but these lead to about the same value for E_0.

It should be noted that the treatment of polar modes that leads to (3.1a) or (3.1b) is correct only for wave functions with s symmetry and therefore becomes less accurate for energies some distance from the band edge. The admixture of p functions that occurs causes a decrease in the matrix element and therefore in the effectiveness of the polar scattering.[14] This effect has been neglected here. The neglect will lead to an overestimate of the effect of polar scattering for large ε, but since, as will be seen, polar scattering is not predominant at large ε, this is not serious.

A plot of τ_{p0} from (3.1b), evaluated using the constants of Table I, is shown as a function of $\varepsilon/\hbar\omega_l\equiv x$ in Fig. 1. As compared with its value for the parabolic case,[15] τ_{p0} is somewhat reduced, by about 20% at $x=10$, 35% at $x=20$. It continues to increase, however, with increasing energy, at least within the range where γ is described by the constants valid for the edge of the conduction band.

The rate of energy loss to polar modes for a nonparabolic band can be derived by the same procedure as used in the Appendix to calculate the collision operator. In fact, the probabilities per unit time of emission and absorption of an optical phonon by an electron with wave vector $\mathbf{k}$ are given by the last two terms, respectively, of Eq. (A1) after division by $-f(\mathbf{k})$. Since $f(\mathbf{k})$ is a constant for the integration, the rates of emission and absorption are just the coefficients of $-f^{(1)}(\varepsilon)$ in Eq. (A7), the expression after integration. This gives for the rate of change of electron energy due to polar

TABLE I. Numerical values used in calculations.

$\hbar\omega_l=0.036$ eV[a]	$\omega_{jj'}=0.7\ \omega_l$[c]
$E_0=5.95\times10^3$ V/cm[b]	$m_2^{(N)}=1.2m_0$[a,b]
$m_1=0.072m_0$[a]	$m_2=0.36m_0$[b]
$E_1(\Gamma_1)=6$ eV[a]	$E_1(X_1)=6\sqrt{2}$ eV[b]
$\alpha=0.576$/eV[b]	$\rho=5.31$ g/cm^3[d]
$\varepsilon_{02}=0.36$ eV[a]	$u_l=5.22\times10^5$ cm/sec[e]
$\omega_{12}=0.8\ \omega_l$[c]	

[a] H. Ehrenreich, Phys. Rev. **120**, 1951 (1960).
[b] See text for discussion.
[c] G. Dolling and J. L. T. Waugh, in *Proceedings of the 1963 International Conference on Lattice Dynamics, Copenhagen, Denmark* (Pergamon Press, New York, 1965), p. 19.
[d] P. Aigrain and M. Balkanski, *Selected Constants Relative to Semiconductors* (Pergamon Press, New York, 1961).
[e] E. Haga and K. Kimura, J. Phys. Soc. Japan **19**, 658 (1964).

[14] H. Ehrenreich, J. Phys. Chem. Solids **9**, 129 (1959).
[15] For a plot of this see Ref. 2.

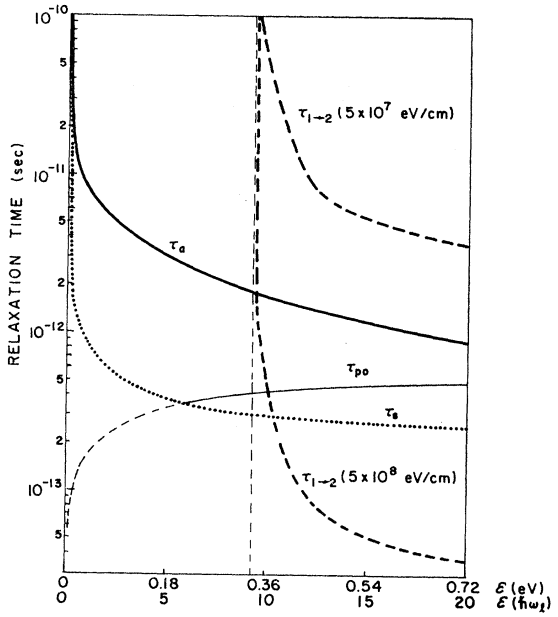

FIG. 1. Relaxation times for scattering of electrons in the (0,0,0) valley of GaAs, corrected for nonparabolicity, as a function of energy.

mode interactions in a nonparabolic band

$$\left(\frac{d\varepsilon}{dt}\right)_{p0}=\frac{eE_0\hbar\omega_l}{[2m_1\gamma(\varepsilon)]^{1/2}}\left[N_{ql}\Omega_1(\varepsilon+\hbar\omega_l)\left(\frac{d\gamma}{d\varepsilon}\right)\Big|_{\varepsilon+\hbar\omega_l}-(N_{ql}+1)\Omega_1(\varepsilon)\left(\frac{d\gamma}{d\varepsilon}\right)\Big|_{\varepsilon-\hbar\omega_l}\right],\quad(3.3)$$

where

$$\Omega_1(\varepsilon)=\ln\left[\frac{\gamma^{1/2}(\varepsilon-\hbar\omega_l)+\gamma^{1/2}(\varepsilon)}{|\gamma^{1/2}(\varepsilon-\hbar\omega_l)-\gamma^{1/2}(\varepsilon)|}\right].\quad(3.4)$$

When $\gamma(\varepsilon)$ is replaced by ε the expression (3.3) goes over to that given earlier for the parabolic case.

Under the assumption of parabolic bands the rate of energy loss of electrons to polar modes in GaAs was found to increase initially as ε increased, reach a maximum at about $5\hbar\omega_l$, and then to decrease slowly as the energy increased beyond that.[16] It was commented that the decreasing effectiveness of polar scattering, evidenced by the increase in τ_{p0} and decrease in $|(d\varepsilon/dt)_{p0}|$ with increasing ε, was responsible for the relatively large number of high-energy electrons at low fields, i.e., for the relatively low threshold for the Gunn effect. Numerical evaluation of (3.3) shows that, although $(d\varepsilon/dt)_{p0}$ is much the same as for the parabolic case up to $\varepsilon=5\hbar\omega_l$, it does not decrease afterward but remains essentially constant. (Perhaps if decrease of the matrix element with increasing ε were taken into account it would still decrease in the range $10\hbar\omega_l\geq\varepsilon\geq5\hbar\omega_l$.) It is

[16] E. M. Conwell, Phys. Rev. **143**, 657 (1966).

clear then, as pointed out by Matz[17] and Dykman and Tomchuk,[18] that the distribution is expected to be cooler when nonparabolicity is taken into account. As will be seen, this was indeed found to be the case.

The proportionality to $\varepsilon^{1/2}$ or $\gamma^{1/2}$ results in τ_{p0} of (3.1a) or (3.1b) getting very small as $\varepsilon \to 0$, and use of these relations undoubtedly overestimates greatly the effect of polar scattering on slow electrons. In actuality, however, such electrons are predominantly scattered by ionized impurities for which the relaxation time τ_I decreases as ε decreases. For slow electrons, because of the logarithmic term,[19] τ_I increases with ε less rapidly than $\varepsilon^{3/2}$, and an $\varepsilon^{1/2}$ dependence should provide at least a fair approximation. (It must be remembered that such slow electrons will make little contribution to the current in any case.) Thus use of τ_{p0} from (3.1a) or (3.1b) as a relaxation time over the entire energy range would have the effect of simulating some impurity scattering in addition to the polar scattering. The calculation using τ_{p0} as the relaxation time for all ε gave a low-field mobility μ_0 of 6200 cm^2/V sec, whereas for pure GaAs, using a variational method, Ehrenreich obtained 9300 cm^2/V sec.[9] The 6200 cm^2/V sec is the value that would be obtained for an impurity concentration of 5×10^{16}/cm^3, a fairly typical value for GaAs samples used in Gunn-effect investigations. It should be noted that impurity scattering is unimportant for high electron energies and therefore for high fields. Thus, beginning at fields not far past the Gunn threshold, the variation of current with field should be independent of impurity concentration.

Intravalley acoustic mode scattering has a relaxation time given for simple band structure by[19]

$$\frac{1}{\tau_a}=\frac{\sqrt{2}}{\pi}\frac{E_1^2 m^{3/2} k_0 T(\varepsilon-\varepsilon_0)^{1/2}}{\hbar^4 \rho u_l^2}\equiv\frac{[2(\varepsilon-\varepsilon_0)/m]^{1/2}}{l_a}, \quad (3.5a)$$

the last equality defining l_a, the mean free path for acoustic deformation potential scattering. Here E_1 is the deformation potential, ρ the density of the crystal, and u_l the velocity of longitudinal acoustic waves. For a nonparabolic band of the type we consider, with $\varepsilon_0=0$, it is found that [20,21]

$$(1/\tau_a)=(2\gamma/m_1)^{1/2}(d\gamma/d\varepsilon)1/l_a. \quad (3.5b)$$

A plot of τ_a from (3.5b) as a function of energy for the central valley, with the numerical values of Table I, is shown in Fig. 1. As compared with the parabolic case,[15] the acoustic scattering is more effective, τ_a being decreased by some 30% at $x=10$, by more than 50% at $x=20$. However, the acoustic scattering remains relatively ineffective for momentum relaxation below $x=10$. Above $x=10$, τ_a comes closer to being comparable to τ_{p0}, but, as will be seen, is still unimportant compared to intervalley scattering. Since the acoustic scattering is also much less effective than polar optical scattering for energy relaxation, it was not included in the calculations for the central valley.

Piezoelectric and nonpolar optical scattering may also be dismissed from consideration for the central valley.[9] It would appear then that polar and impurity scattering are the only processes of importance for energies below that for which transitions to the ⟨100⟩ valleys become possible. However, as pointed out earlier,[22,5] the very considerable scatter in room-temperature mobilities, with μ_0 typically 5000 to 6000 cm^2/V sec in samples for which a combination of polar and impurity scattering would predict $\mu_0\sim8000$ cm^2/V sec, combined with the fact that the scatter in μ_0 is less at 78°, point to the operation of another scattering process. From an analysis of the temperature dependence of μ_0, Weisberg has concluded that the additional process, termed by him a "mobility killer," has a characteristic mobility μ_s proportional to $T^{-1/2}$ or $T^{-3/4}$.[22] In InP, where similar phenomena have been found, they have been connected with the presence of an impurity. In the case of GaAs, Weisberg suggests that the "mobility killer" consists of large intrinsic regions arising from compensation of the majority impurity, a shallow donor, by a randomly distributed deep-lying acceptor. It is not unlikely that such acceptor impurities are present in typical boat- or melt-grown samples in concentrations as high as 10^{16}/cm^3.[23] The intrinsic region will include not only the portion of material that is compensated, but a space-charge region that forms around it to provide the appropriate potential difference with respect to the uncompensated material or matrix. For samples with carrier concentration $n\simeq10^{15}$/cm^3 and greater, this difference in potential is almost one-half the energy gap. The size of the intrinsic region, including the space-charge, varies from close to that of the compensated region itself in material with high n, to many times larger in material with low n. A size of 200 Å or more is not unreasonable in samples with $n\simeq10^{15}$/cm^3. Despite the very large size that such regions might attain in high-resistivity material, their scattering effect would not be large there because the potential step or barrier between them and the surrounding material would be small. Thus the maximum scattering effect of these intrinsic regions is expected to be in material with $10^{16}\leq n\leq10^{14}$/cm^3. In samples with n in the range 10^{15} to 10^{16}/cm^3, for example, due to the large dimensions that can reasonably be expected, and a barrier height

[17] D. Matz, Solid State Commun. 4, 491 (1966); J. Phys. Chem. Solids 28, 373 (1967).
[18] I. M. Dykman and P. M. Tomchuk, Fiz. Tverd. Tela 8, 1343 (1965) [English transl.: Soviet Phys.—Solid State 8, 1075 (1966)].
[19] See, for example, P. P. Debye and E. M. Conwell, Phys. Rev. 93, 693 (1954).
[20] L. Sosnowski, in *Physics of Semiconductors* (Academic Press Inc., New York, 1964), p. 341.
[21] J. Kolodziejczak, Phys. Status Solidi 19, 231 (1967).
[22] L. R. Weisberg, J. Appl. Phys. 33, 1817 (1962).
[23] L. R. Weisberg, F. D. Rosi, and P. G. Herkart, *Properties of Elemental and Compound Semiconductors* (Interscience Publishers, Inc., New York, 1960), p. 25.

almost half the gap, such regions would be essentially opaque to electrons with $\varepsilon \leq 0.5$ eV.

This discussion suggests treating the intrinsic regions as impenetrable spheres of density N_s and scattering cross section Q. For the simple model of band structure, one then obtains a relaxation time for the space-charge scattering, as this process is also called,

$$\tau_s = (N_s Q v)^{-1} = (N_s Q)^{-1}[m/2(\varepsilon - \varepsilon_0)]^{1/2}. \quad (3.6)$$

For a Maxwell-Boltzmann distribution at the lattice temperature this leads to a mobility μ_s given by

$$\mu_s = 4e/3N_s Q(2\pi m k_0 T)^{1/2} = 2.4\times 10^9/N_s Q(Tm/m_0)^{1/2} \text{ cm}^2/\text{V sec}, \quad (3.7)$$

which has a $T^{-1/2}$ dependence, more or less in agreement with experimental observations for the mobility killer. The $T^{-1/2}$ dependence of μ_s, or more exactly the v^{-1} dependence of τ_s, means that, unlike impurity scattering, as the average electron energy is rasied this process becomes more important. It is also clear from this that one need consider it only for the light electrons in the field range with which we are concerned. To take it into account in the calculations, one would obtain a typical value of $N_s Q$ by determining the amount of μ_s required to reduce μ_0 to a typical value, say 5500 cm^2/V sec, from the theoretical value for combined polar optical and impurity scattering. This procedure has been followed for some of the calculations to be described here. In Fig. 1 is shown τ_s versus ε for $N_s Q = 3.2\times 10^4$ cm^{-1}, which leads to $\mu_0 \simeq 5500$ cm^2/V sec for a sample with 10^{15} impurities per cm^3. For this plot v has been corrected for the nonparabolicity of the central valley, i.e., τ_s was calculated from

$$\tau_s = (N_s Q)^{-1}(m_1/2\gamma)^{1/2} d\gamma/d\varepsilon, \quad (3.8)$$

rather than from (3.6). The plot overestimates the effect of this mechanism for $\varepsilon \geq 0.5$ eV, or $x \geq 14$, since, as indicated earlier, this is the order of magnitude of the barrier height. The error will not be significant in the present calculations, however, for intervalley scattering is more important at such high energies.

It should be noted, however, that if this is indeed the mechanism for the additional scattering there would also be a distortion of the lines of current flow by these opaque regions. This would also lead to a reduction in mobility, and in fact one that could be larger than the reduction due to the decrease in mean free path. To determine this it would be necessary to know more about the size and distribution of the space-charge regions. Incorporation of τ_s into the calculations as described can only be considered a crude attempt to take this mechanism into account.

When the energy of a carrier is high enough the carrier can make a transition from the (000) valley to one of the ⟨100⟩ valleys. Conservation of crystal momentum requires that in the process, for the moderately doped samples considered here, a phonon with wave vector at the edge of the Brillouin zone, and directed along ⟨100⟩, be emitted or absorbed. Since the ⟨100⟩ minima occupied by the electrons have X_1 symmetry, the selection rules dictate that the phonons involved must have this symmetry also.[24] In GaAs this means that they must be the longitudinal optical (LO) phonons at the edge of the Brillouin zone.[24] The energy of these phonons is 0.8 $\hbar\omega_l$, corresponding to a characteristic temperature of 330°.[25]

Intervalley scattering does have a relaxation time, the general expression for which is given by Eq. (A.23) in the Appendix. For the (0,0,0) valley, after the use of (A.19b), this relaxation time is found to be

$$\frac{1}{\tau_{1\to 2}^{(1)}} = \frac{D_{12}^2 (m_2^{(N)})^{3/2}}{2^{1/2}\pi\hbar^3\rho\omega_{12}} \frac{1}{e^{x_{12}}-1} [(\varepsilon+\hbar\omega_{12}-\varepsilon_{02})^{1/2} + e^{x_{12}}(\varepsilon-\hbar\omega_{12}-\varepsilon_{02})^{1/2}], \quad (3.9)$$

where D_{12} is the coupling constant, ω_{12} the angular frequency for transitions between the (000) valley (denoted by the index 1) and a ⟨100⟩ valley (denoted by the index 2) and $x_{12} = \hbar\omega_{12}/k_0 T$. As discussed in the Appendix $\tau_{1\to 2}^{(1)}$ is unaffected by the departure from parabolicity of the (0,0,0) valley. If we take the edge of the conduction band as the zero of our energy scale, $\varepsilon_{02} = 0.36$ eV. The quantities $m_2^{(N)}$, ω_{12}, and ρ are known, so the only unknown in (3.9) is D_{12}. It has been suggested, based on the observation (or supposed observation) of low-field avalanche breakdown in GaAs, that $D_{12} \simeq 1\times 10^8$ eV/cm.[26,27] In the calculations we used D_{12} as a parameter, and results for different D_{12} values will be discussed later. As background for understanding these results, we show in Fig. 1 plots of the intervalley relaxation time for D_{12} values of 5×10^7 eV/cm and 5×10^8 eV/cm. It is seen that for the lower value the average time required for a carrier in the central valley to make a transition to a ⟨100⟩ valley would be of the order of 10^{-11} sec. Since Gunn oscillations have been seen at frequencies as high as 40 Gc/sec, 5×10^7 eV/cm would seem to be close to the lower limit for D_{12}. It is noteworthy that for 5×10^7 eV/cm polar scattering remains predominant throughout, while for 5×10^8 eV/cm intervalley scattering is predominant over almost the entire range in which it is energetically possible. D_{12} in the range 1 to 2×10^8 eV/cm represents an intermediate case, with the two processes comparable in importance.

4. TRANSPORT IN THE UPPER VALLEYS

Less is known about transport in the upper valleys than in the lower. Measurements under hydrostatic pressure have yielded low-field mobility values of 155

[24] J. L. Birman, M. Lax, and R. Loudon, Phys. Rev. **145**, 620 (1966).
[25] G. Dolling and J. L. T. Waugh, in *Proceedings of the International Conference on Lattice Dynamics, Copenhagen, 1963* (Pergamon Press, Inc., New York, 1965), p. 19.
[26] J. A. Copeland, Appl. Phys. Letters **9**, 140 (1966).
[27] E. M. Conwell, Appl. Phys. Letters **9**, 383 (1966).

cm²/V sec (Ref. 28) and 110 cm²/V sec (Ref. 29). A value of about 170 cm²/V sec was obtained by extrapolation to $x=1$ of Hall mobilities measured on a set of $GaAs_xP_{1-x}$ alloys.[30]

At the time most of our earlier calculations were done, the deformation potential for intravalley acoustic scattering was not known and we assumed the same value for the upper valleys as for the lower. Since that time measurements under uniaxial pressure have yielded the values[31] $\alpha_1=\Xi_d+\Xi_u=10.3$ eV and $\alpha_2=\Xi_d=7.0$ eV. From these we deduce $\Xi_u=3.3$ eV. For ellipsoidal constant energy surfaces the relaxation time for intravalley acoustic mode scattering is no longer independent of direction, but may, unless the anisotropy is severe, be represented by a tensor with components in the three principal directions for a given valley[32]

$$\frac{1}{\tau_\alpha}=\frac{2^{1/2}\Xi_\alpha^2\bar{m}^{3/2}k_0T}{\pi\hbar^4c_l}(\varepsilon-\varepsilon_0)^{1/2}, \tag{4.1}$$

where α stands for longitudinal (l) or transverse (t) and c_l is an average elastic constant for longitudinal waves ($\simeq\rho u_l^2$). Ξ_α is a deformation potential constant, defined by

$$\Xi_\alpha^2=0.75[\xi_\alpha\Xi_d^2+\eta_\alpha\Xi_d\Xi_u+\zeta_\alpha\Xi_u^2], \tag{4.2}$$

where ξ_α, η_α, and ζ_α are functions of m_t/m_l tabulated by Herring and Vogt.[32] Since the ratio m_t/m_l should have about the same value for the ⟨100⟩ minima of GaAs as it has for these minima in Si, and further since Ξ_α varies slowly with this ratio, we shall use the values of ξ_α, η_α, and ζ_α calculated for silicon.[32] These, with the values of Ξ_d and Ξ_u given above, lead to $\Xi_l^2=107$ eV, $\Xi_t^2=78$ eV. With these numbers we see that the anisotropy is not severe, τ_t being about 40% larger than τ_l.

The mobility for the many-valley model is given by[32]

$$\mu=\frac{e}{3m_l}\frac{\langle(\varepsilon-\varepsilon_0)\tau_l\rangle}{\langle\varepsilon-\varepsilon_0\rangle}+\frac{2}{3m_t}\frac{\langle(\varepsilon-\varepsilon_0)\tau_t\rangle}{\langle\varepsilon-\varepsilon_0\rangle}. \tag{4.3}$$

Using (4.1) for the τ's and evaluating the indicated averages, we obtain the mobility

$$\mu_a=\frac{4el_{a1}}{3(2\pi m_tk_0T)^{1/2}}\left[\frac{1}{3}\left\{\frac{m_t}{m_l}\frac{\Xi_d^2}{\Xi_l^2}+\frac{2\Xi_d^2}{\Xi_t^2}\right\}\right], \tag{4.4}$$

where l_{a1} is a generalized mean free path defined by

$$l_{a1}=\frac{\pi\hbar^4c_l}{\bar{m}^{3/2}m_t^{1/2}\Xi_d^2k_0T}. \tag{4.5}$$

With the numbers given earlier for Ξ_d and Ξ_u, and $m_t=0.23m_0$, $m_l=1.3m_0$, (4.4) gives $\mu_a\simeq1400$ cm²/V sec.

It is noted that if we allow the many-valley model to go over into the simple model by setting $m_l=m_t=m$, $\Xi_u=0$, and $\Xi_d=E_1$, l_{a1} goes over to the mean free path for the simple model, given by (3.5a), the angular bracket in (4.4) goes to unity, and μ_a goes over to the mobility under deformation potential scattering in the simple model. To obtain $\mu_a=1400$ cm²/V sec in the simple model with $m=0.36m_0$, the value we used in earlier calculations,[2–6] would require $E_1^2=72$ eV², twice as large as the value used earlier.

To obtain an estimate of the importance of polar mode scattering, we assume that the matrix element[14] has the same value for the ⟨100⟩ valleys as for (000). In any case the matrix element can be no larger than it is for that case. An investigation of scattering by polar modes in the many-valley model[33] has led to the conclusion that a good approximation to the correct polar mobility μ_{po} may be obtained by replacing the factor $m^{-3/2}$ that appears in μ_{po} for the simple model by $\bar{m}^{-1/2}\times(1/3m_l+2/m_t)$. With $m_t=0.23m_0$, $m_l=1.3m_0$, the factor in parenthesis, which is the reciprocal of the inertial mass, is $0.32m_0$, while $\bar{m}$ is $0.41m_0$. This leads to a μ_{po} value for an X_1 valley which is μ_{po} for the Γ_1 valley, 10 000 cm²/V sec, multiplied by $(0.072)^{3/2}/(0.41)^{1/2}\times(0.32)$, or 900 cm²/V sec. If the masses are actually larger, as indicated earlier might be the case, μ_{po} could be somewhat smaller, but it is still well above the observed upper-valley mobility.

Another scattering process that must be considered for the X_1 valleys is scattering of electrons to the Γ_1 valley. The relaxation time $\tau_{2\to1}^{(2)}$ for this process is obtained by inserting (A19a) in the general expression (A23), which gives

$$\frac{1}{\tau_{2\to1}^{(2)}}=\frac{D_{12}^2m_1^{3/2}}{2^{1/2}\pi\hbar^3\rho\omega_{12}}\frac{1}{e^{x_{12}}-1}[\gamma^{1/2}(\varepsilon+\hbar\omega_{12})\gamma'(\varepsilon+\hbar\omega_{12})+e^{x_{12}}\gamma^{1/2}(\varepsilon-\hbar\omega_{12})\gamma'(\varepsilon-\hbar\omega_{12})]. \tag{4.6}$$

Even with the effects of nonparabolicity included, the density of states in the central valley is so small that $\tau_{2\to1}^{(2)}$ is much larger than the τ's for acoustic mode or polar optical scattering,[34] and this process is unimportant in limiting the mobility in the X_1 valleys.

It is seen that a combination of the three processes already considered for the upper valleys gives a mobility well above the observed value, and that another scattering process must be operative, in fact predominant. Since equivalent intervalley scattering is known to be important in silicon,[35] it is likely to be so here too. The relaxation time for scattering between ⟨100⟩ valleys, to

[28] G. King, J. Lees, and M. P. Wasse, quoted by P. N. Butcher and W. Fawcett, Phys. Letters **21**, 489 (1966).
[29] A. R. Hutson, A. Jayaraman, and A. S. Coriell, Phys. Rev. **155**, 786 (1967).
[30] M. Shyam, Stanford University (private communication).
[31] M. Shyam, J. W. Allen, and G. L. Pearson, Trans. IEEE **ED-13**, 63 (1966)
[32] C. Herring and E. Vogt, Phys. Rev. **101**, 944 (1956).
[33] D. J. Olechna and H. Ehrenreich, J. Phys. Chem. Solids **23**, 1513 (1962).
[34] For a plot of the relaxation times in the X_1 valley versus energy see Ref. 2. Note, however, that τ_{ac} should be reduced by a factor 2 because E_1^2 is twice as large as assumed there.
[35] D. Long, Phys. Rev. **120**, 2024 (1960).

be denoted by $\tau_{j\to j'}$, may also be obtained from the general expression (A23). For the case of the minima at the edge of the Brillouin zone, transitions between valleys at opposite ends of the same cube axis require no phonon at all, while those between valleys on different cube axes require the LO phonon at the zone edge in the ⟨100⟩ direction.[24] (In this case the crystal momenta add up to a reciprocal lattice vector rather than zero.) This phonon, with angular frequency $\omega_{jj'}=0.8\omega_l$,[25] is the same as that required for the Γ_1 to X_1 transition. Denoting the coupling for this process by $D_{jj'}$, we obtain from (A19b) and (A23)

$$\frac{1}{\tau_{j\to j'}}=\frac{2}{3}\frac{D_{jj'}{}^2(m_2{}^{(N)})^{3/2}}{2^{1/2}\pi\hbar^3\rho\omega_{jj'}}\frac{1}{e^{x_{jj'}}-1}$$
$$\times[(\varepsilon+\hbar\omega_{jj'}-\varepsilon_{02})^{1/2}+e^{x_{jj'}}(\varepsilon-\hbar\omega_{jj'}-\varepsilon_{02})^{1/2}], \quad (4.7)$$

For the calculations we have taken for $D_{jj'}$ the value derived from Long's results for equivalent intervalley scattering in Si, 1×10^9 eV/cm.[4] It is apparent that even with the same coupling constant intervalley scattering would be more important for GaAs than for Si because of the smaller size of the phonons.[4] This is borne out by the fact that τ for this process, with $D_{jj'}=1\times10^9$ eV/cm, is much smaller than the τ's considered above,[34] and μ_0 for the X_1 valleys calculated including $\tau_{j\to j'}$ came out 145 cm²/V sec.

Because the mobility is already so small, impurity scattering and space-charge scattering may be neglected for the upper valleys.

5. BOLTZMANN EQUATION FOR THE LOWER VALLEY

We consider in this section the solution of the Boltzmann equation for $\varepsilon<\varepsilon_{02}-\hbar\omega_{12}$, i.e., energies too low for electrons in the central valley to make transitions to the outer valleys. As discussed in Sec. 3, the only scattering processes that need then be considered are polar optical scattering and, in material with the appropriate inhomogeneity, space-charge scattering. We take up first the case of ideal material.

For arbitrary fields the distribution function f may be expanded in a series of Legendre polynomials:

$$f=\sum_{n=0}^{\infty} f_n(\varepsilon)P_n(\cos\theta), \quad (5.1)$$

where θ is the angle between $\mathbf{k}$ and $\mathbf{E}$, the electric field. Insertion of (5.1) into the Boltzmann equation leads to an infinite set of coupled differential equations for the f_n's,[36] i.e., an intractable problem.[37] Fortunately, of course, the set of equations may be truncated in low fields, and in high fields for which the scattering is reasonably elastic and isotropic, by setting $f_n=0$ for $n\geq2$. The distribution that results is essentially an isotropic one with a small drift or streaming term superimposed. Such a distribution is not appropriate for high fields, however, when the scattering is predominantly inelastic. In that case the distribution is quite anisotropic, with a strong streaming in the force direction. A method of truncating the infinite set of coupled equations appropriate to this case has been suggested by Baraff.[36] In this method, called the maximum-anisotropy approximation, f_n's for $n\geq N$, a value chosen arbitrarily, are replaced by the values they would have for the distribution of maximum anisotropy, a distribution in which all carirers are traveling in the force direction.

In the light of this discussion, the approximation of dropping all terms beyond $n=1$ in the expansion (5.1), i.e., taking

$$f=f_0+f_1\cos\theta\equiv f_0+k_E g(\varepsilon), \quad (5.2)$$

where k_E is the component of $\mathbf{k}$ along the field direction, should be good for GaAs at low fields, and at fields high enough so that $\langle\varepsilon\rangle\gg\hbar\omega_l$. Calculating with (5.2) we have found that $\langle\varepsilon\rangle\simeq3\hbar\omega_l$ at a field of 3 or 4 kV/cm, depending on the parameters used. Thus the polar scattering is certainly inelastic for the majority of electrons at fields less than 3 or 4 kV/cm. However, there is also elastic scattering present in the form of impurity, acoustic, and space-charge scattering. The elastic scattering will oppose the streaming tendency and tend to randomize the distribution. Impurity scattering would be the most effective here since it affects predominantly the slow electrons, for which the streaming tendency would be greatest. Thus in the range of fields for which $\hbar\omega_l\leq\langle\varepsilon\rangle\leq3\hbar\omega_l$ the correct distribution lies between the extremes represented by (5.2) and the maximum-anisotropy approximation. As noted earlier, our calculations have been carried out using (5.2) at all fields. Stenflo[38] has carried out some calculations for GaAs using the maximum anisotropy approximation with $N=2$. The results will be compared in Sec. 8.

It is, of course, true that even in high fields, (5.2) provides a poor description of the distribution of the low-energy electrons.[39] However, this is unimportant because these are relatively few in number, and their contribution to the current is quite small.

In setting up the Boltzmann equation, it is convenient to work with the dimensionless variable

$$x\equiv\varepsilon/\hbar\omega_l, \quad (5.3)$$

[36] G. Baraff, Phys. Rev. **133**, A26 (1964).

[37] A neat method for circumventing this has, however, been found by H. Budd {in *Proceedings of the International Conference on the Physics of Semiconductors, Kyoto, 1966* [J. Phys. Soc. Japan Suppl. **21**, 420 (1966)]} and applied to the case of inelastic scattering by nonpolar optical modes. This method requires that there exist a generalized low-field relaxation time, i.e., that the rate of change of f_n due to collisions satisfy the condition $(\partial f_n/\partial t)_c=-f_n/\tau$ for $n\geq1$. Unfortunately, this condition is not satisfied by the polar modes.

[38] L. Stenflo, Proc. IEEE **55**, 1088 (1967). We are indebted to Dr. Stenflo for a preprint of his manuscript.

[39] L. Stenflo, Proc. IEEE **54**, 1970 (1966).

and to replace $\gamma(\varepsilon)$ by the dimensionless function

$$\Gamma(x)=\gamma(\hbar\omega_l x)/\hbar\omega_l=x+\alpha\hbar\omega_l x^2+\cdots. \quad (5.4)$$

The calculations will be carried out for the nonparabolic case only. The results for the parabolic case are easily obtained by setting $\Gamma=x$, $\Gamma'=1$. To avoid cumbersome notation in what follows, we shall denote the distribution for the lower valley by $f^{(1)}$, its spherically symmetric part [f_0 of Eq. (5.3)] by f_1, and its asymmetric part by $k_E g_1$. With this notation the rate of change of the distribution due to acceleration by the field takes the form

$$\left[\frac{\partial f^{(1)}}{\partial t}\right]_E=-\frac{eE}{\hbar}\cdot\nabla_k f^{(1)}=-\frac{eE}{\hbar}\times\left(g_1+\frac{2}{3}\frac{\Gamma}{\Gamma'}g_1'+\frac{\hbar^2k_E}{m_1\Gamma'\hbar\omega_l}f_1'\right), \quad (5.5)$$

where the prime indicates differentiation with respect to x. An approximation similar to that usually made for the parabolic case has been made here in replacing $\hbar^2k_E^2/m_1$ by its average, $\frac{1}{3}2\Gamma$, in the second term. The collision term will be simplified by assuming that a collision time τ exists, which makes it possible to write

$$[\partial f^{(1)}/\partial t]_c=(\partial f_1/\partial t)_c+(\partial k_E g_1/\partial t)_c=(\partial f_1/\partial t)_c-(k_E g_1/\tau). \quad (5.6)$$

When scattering is by the polar modes we insert for τ in (5.6) the τ_{po} of (3.1b), or more exactly, (A13). As discussed in Sec. 3, although this is not correct for the polar modes unless $\varepsilon\gg\hbar\omega_l$, it does represent a good over-all approximation for a sample with a moderate amount of impurity scattering. In any case, it should be a good approximation for fields of several thousand V/cm and higher.

The vanishing of $[\partial f^{(1)}/\partial t]_E+[\partial f^{(1)}/\partial t]_c$ implies that terms in different powers of k_E vanish separately. The Boltzmann equation is then equivalent to the pair of equations

$$-\frac{2eE}{3\hbar\Gamma'\Gamma^{1/2}}\frac{d}{dx}(\Gamma^{3/2}g_1)+\left(\frac{\partial f_1}{\partial t}\right)_c=0 \quad (5.7)$$

and

$$-\frac{heE}{m_1\Gamma'\hbar\omega_l}f_1'-\frac{g_1}{\tau^{(1)}}=0, \quad (5.8)$$

where $\tau^{(1)}$ is the relaxation time for the (000) valley. From the last equation we obtain

$$g_1=-\frac{heE\tau^{(1)}}{m_1\hbar\omega_l\Gamma'}f_1'. \quad (5.9)$$

When (5.9) is inserted into (5.7) we obtain the differential equation that must be solved for the lower valley:

$$\frac{2e^2E^2}{3m_1\hbar\omega_l\Gamma'\Gamma^{1/2}}\frac{d}{dx}\left(\frac{\Gamma^{3/2}}{\Gamma'}\tau^{(1)}f_1'\right)+\left(\frac{\partial f_1}{\partial t}\right)_c=0. \quad (5.10)$$

When scattering is by polar modes (and impurities) only, $\tau^{(1)}$ is, as noted earlier, given by (A13) and $(\partial f_1/\partial t)_c$ by (A9) rewritten in terms of x, i.e.,

$$\left(\frac{\partial f_1}{\partial t}\right)_{po}=\frac{eE_0}{(2m_1\hbar\omega_l\Gamma(x))^{1/2}}\frac{1}{e^{x_l}-1}\{[e^{x_l}f_1(x+1)-f_1(x)]\times\Omega(x+1)\Gamma'(x+1)+[f_1(x-1)-e^{x_l}f_1(x)]\times\Omega(x)\Gamma'(x-1)\}, \quad (5.11)$$

where

$$\Omega(x)=\ln\left[\frac{\Gamma^{1/2}(x-1)+\Gamma^{1/2}(x)}{|\Gamma^{1/2}(x-1)-\Gamma^{1/2}(x)|}\right]. \quad (5.12)$$

To simplify the solution of (5.10) for this case, we expand $f_1(x\pm1)$ in a Taylor series about x and drop terms past $f_1''(x)$. Again, this approximation should be good when $\langle\varepsilon\rangle\gg\hbar\omega_l$. The second-order differential equation that results must be integrated numerically except for quite large values of E, to be considered later. This means that values of $f_1(0)$ and $f_1'(0)$ must be chosen to begin the integration. The value of the former is arbitrary since the differential equation is homogeneous. Ultimately, of course, $f_1(0)$ will be determined by normalization. Carrying out the integration for different values of $f_1'(0)$, one finds that solutions well-behaved out to large x may be obtained for a wide range of values of $f_1'(0)$ at each field. The following procedure was used to determine which value is correct for the particular boundary conditions of the present problem. If Eq. (5.10), with (A13) and (5.11) inserted, is integrated once before expansion of $f_1(x\pm1)$, we obtain

$$C=a\left(\frac{\Gamma}{\Gamma'}\right)^2f_1'+\frac{1}{e^{x_l}-1}\int_0^x\Gamma'(y)\times\{[e^{x_l}f_1(y+1)-f_1(y)]\Omega(y+1)\Gamma'(y+1)+[f_1(y-1)-e^{x_l}f_1(y)]\Omega(y)\Gamma'(y-1)\}dy, \quad (5.13)$$

where C is the constant of integration and

$$a=\frac{4}{3}\frac{E^2}{E_0^2}\frac{e^{x_l}-1}{e^{x_l}+1}. \quad (5.14)$$

Equation (5.13) is true for all x, hence for $x=0$. As $x\to0$, $\Gamma'(x)$ and $\Gamma'(x\pm1)\to1$, $\Omega(x+1)\to2\sinh^{-1}x^{1/2}$, and $\Gamma'(x)$ times the quantity in the angular bracket is well-behaved. [Note that the term in $\Omega(x)$ is not to be included unless $x\geq1$.] This has the consequence that the integral vanishes as $x\to0$. Since $\Gamma(x)\to0$ and $f_1'(0)$ must be finite, we conclude that $C=0$. In the absence of an analytic solution of (5.13) this condition cannot

be used in the usual way to determine the correct $f_1'(0)$. It can, however, be made use of in the following way. For $x\gg1$, $\Omega(x)$, $\Omega(x+1)$ and $\Gamma'(x\pm1)$ may be expanded as well as $f_1(x\pm1)$, and the collision operator takes the form (A11). It is easily shown that (A11) may be written

$$\left(\frac{\partial f_1}{\partial t}\right)_{po} \underset{x\gg1}{\rightarrow} \frac{eE_0}{(2m_1\hbar\omega_l\Gamma)^{1/2}}\frac{1}{\Gamma'}\frac{d}{dx}\left[\frac{1}{2}\frac{e^{xl}+1}{e^{xl}-1}-(\Gamma')^2 \times\ln\left(\frac{4\Gamma}{\Gamma'}\right)f_1'+(\Gamma')^2\ln\left(\frac{4\Gamma}{\Gamma'}\right)f_1\right]. \quad (5.15)$$

When (5.15) is inserted into the differential equation (5.10) the result can be integrated once to give the equation valid for large x:

$$\left[a\Gamma^2+d(\Gamma')^4\ln\left(\frac{4\Gamma}{\Gamma'}\right)\right]f_1'+(\Gamma')^4\ln\left(\frac{4\Gamma}{\Gamma'}\right)f_1=0, \quad (5.16)$$

where a was defined by Eq. (5.14) and $d=(e^{xl}+1)/2(e^{xl}-1)$. The condition $C=0$ has already been inserted. For a given value of x, say $x=b$, Eq. (5.16) is in the form

$$A_1(b)f_1(b)+A_2(b)f_1'(b)=0 \quad (5.17a)$$

or

$$\mathbf{A}(b)\cdot\mathbf{F}(b)=0, \quad (5.17b)$$

where $A_1(b)$ and $A_2(b)$ are thought of as the components of the vector $\mathbf{A}(b)$, and $f_1(b)$ and $f_1'(b)$ the components of the vector $\mathbf{F}(b)$. Because $f_1(x)$ is the solution of a second-order linear differential equation, the vector $\mathbf{F}(b)$ is related linearly to the vector $\mathbf{F}(a)$, i.e.,

$$\mathbf{F}(b)=\mathbf{c}(b,a)\cdot\mathbf{F}(a), \quad (5.18)$$

where $\mathbf{c}$ is the matrix

$$\mathbf{c}(b,a)=\mathbf{W}(b)\cdot\mathbf{W}^{-1}(a), \quad (5.19)$$

$W(\alpha)$ being the Wronskian at $x=\alpha$. If the relation (5.18) for $a=0$ is inserted into (5.17b) we obtain

$$\mathbf{A}(b)\cdot\mathbf{c}(b,0)\cdot\mathbf{F}(0)=0. \quad (5.20)$$

Since the coefficients $\mathbf{A}(b)$ are known and the matrix $\mathbf{c}$ can be determined by numerical integration of the second-order differential equation obtained from (5.10) for any two (different) sets of initial conditions, Eq. (5.20) gives a relation between $f_1(0)$ and $f_1'(0)$ that can be used to select the correct $f_1'(0)$.

The results of numerical integration of Eq. (5.10) with $(\partial f_1/\partial t)_c$ given by (5.11) after replacing $f_1(x\pm1)$ by $f_1\pm f_1'+(1/2)f_1''$ are shown in Fig. 2 for the nonparabolic case and in Fig. 3 for the corresponding parabolic case, i.e., for $\Gamma(x)$ replaced by x, all other quantities remaining unchanged. The values of the various constants used are shown in Table I. The solutions have been plotted down to $x=0$ although accuracy should not be good for small x. Low fields have been included

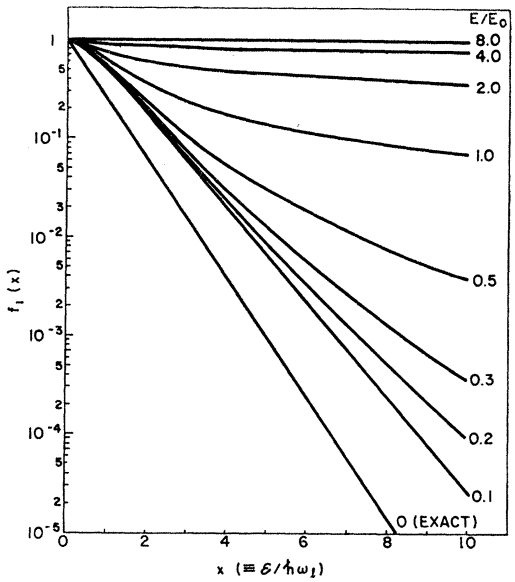

FIG. 2. Distribution functions for electrons in the (0,0,0) valley with nonparabolicity taken into account. The numbers at the right give the electric field intensity in units of $E_0=5.95$ kV/cm.

although, there too, in principle, the solutions should not be very good. The solutions of Fig. 3 differ from those for that case given earlier[2] in that the latter were solutions of the equation obtained by using for all x the form (5.15) valid for large x (with $\Gamma=x$, of course). This resulted in a singularity at small x, which is why those solutions were presented only for $x\geq0.3$.

By comparison of Figs. 2 and 3 it is seen that f_1 is

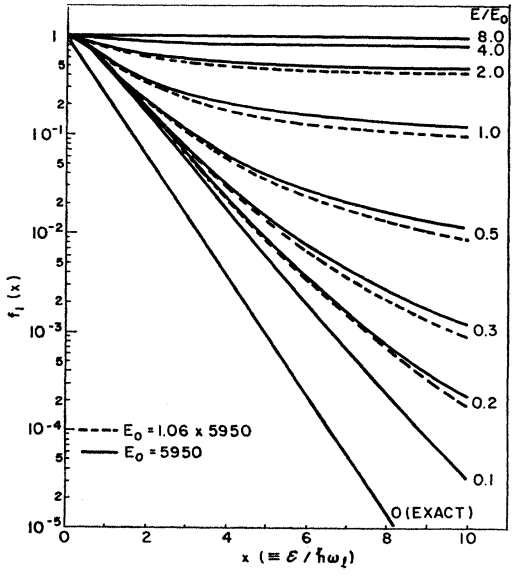

FIG. 3. Distribution functions for electrons in the (0,0,0) valley with nonparabolicity neglected, i.e., $\alpha=0$. The solid lines are for $E_0=5.95$ kV/cm, the dashed lines for $E_0=1.06\times5.95$ kV/cm. The numbers at the right give the electric field intensity in units of 5.95 kV/cm for both cases.

the same for parabolic and nonparabolic cases at small x, where $\Gamma(x)\simeq x$, and that at higher x the nonparabolic f_1 lies below the parabolic one. This is the anticipated cooling of the distribution, and it is particularly large for fields in the range 0.3 to 1.0 E_0. The non-Maxwellian character of the solutions, manifested by their departure from straight lines, is still apparent in the nonparabolic case at fields of 0.3 E_0 and above. As remarked earlier for the parabolic case,[2] the deviation is such as to give relatively fewer low-energy electrons and more high-energy electrons than a Maxwellian of the same $\langle\varepsilon\rangle$. Although this tendency is less marked in the distribution for the nonparabolic case than for the parabolic, that will be offset, so far as actual electron populations in the different energy ranges are concerned, by the higher density of states at high energy in the nonparabolic case.

Beyond $E=0.3E_0$ the differences between the nonparabolic and parabolic distributions are seen to decrease as E increases. This can be understood as follows. From (5.15) we obtain[40]

$$f_1=\exp\left\{-\left[\int\frac{(\Gamma')^4\ln(4\Gamma/\Gamma')}{a\Gamma^2+d(\Gamma')^4\ln(4\Gamma/\Gamma')}dx\right]\right\}. \quad (5.21)$$

For the parabolic case, i.e., $\Gamma=x$, the term $a\Gamma^2\gg d(\Gamma')^4\times\ln(4\Gamma/\Gamma')$ for large x and large E and the latter term may be neglected. Equation (5.21) may then be integrated to give[2]

$$f_1^{\mathrm{P}}=e^{(1/a)G(x)}\equiv e^{(1/a)[(1/x)+(\ln 4x/x)]}, \quad (5.22)$$

where the superscript P indicates parabolic. It can be checked with the use of Fig. 3 that this is actually quite a good approximation for $x\geq 6$ when $E=\frac{1}{2}E_0$, for $x\geq 4$ when $E=E_0$, etc. The dropping of the second term in the denominator for large x is not generally permissible in the nonparabolic case because of the rapid increase of $(\Gamma')^4$ with x. However, it is still a fair approximation in the present case in the neighborhood of $x=10$ and for $E\geq E_0$ to neglect the ln term in the denominator. When this is done, (5.21) for the nonparabolic case takes the form

$$f_1^{\mathrm{NP}}\simeq e^{(1/a)G'(x)}, \quad (5.23)$$

where $G'(x)$ is a function of x and α, but does not depend on E. Since f_1^{P} and f_1^{NP} differ only at large x, where they are relatively small anyway, the normalization constants may be assumed to be the same, and we conclude that

$$\frac{f_1^{\mathrm{P}}}{f_1^{\mathrm{NP}}}\simeq e^{(1/a)[G(x)-G'(x)]}. \quad (5.24)$$

It is readily seen from this that as E increases and therefore a increases the ratio $f_1^{\mathrm{P}}/f_1^{\mathrm{NP}}$ at a given x must decrease.

In Fig. 3 there are shown also, in dotted lines, the results of calculating with an E_0 that is 6% higher than that taken for the other calculations. This decreases f_1 at high x, or cools the distributions, as expected because an increase in E_0 means increased coupling to and scattering by the polar modes.

6. COUPLED BOLTZMANN EQUATIONS AND SOLUTIONS

A convenient way of treating a valley with ellipsoidal constant energy surfaces is to perform a transformation of coordinates in momentum space that makes the ellipsoids spheres. In the transformed space the distribution may be expanded in the form (5.1) with θ representing the angle between the transformed $\mathbf{k}$ and $\mathbf{E}$ vectors.[41] With the use of this transformation solutions of the Boltzmann equation have been found for the $\langle 111\rangle$ valleys of Ge in high fields with the series (5.1) terminated at $n=1$.[42] These solutions were based on the assumption that intervalley scattering is weak. For field directions other than $\langle 100\rangle$ the solutions were in general different for different valleys. The differences among the $n=0$ terms signify different average energies or different temperatures for the different valleys. The temperature is found to depend on the angle between $\mathbf{E}$ and the major axis of the ellipsoids, as expected, because the size of the mass in the field direction is important in determining how effectively the valleys are heated. The $n=1$ terms were also found to be different in magnitude, and were directed differently for the different valleys, in general. When the current density $\mathbf{j}$ is calculated by adding the contributions of the various valleys, in low fields the anisotropy washes out and $\mathbf{j}$ is parallel to $\mathbf{E}$, but in high fields some effect of anisotropy remains and $\mathbf{j}$ is found to be at an angle to $\mathbf{E}$.

The problem has not been solved in high fields for the case of strong equivalent intervalley scattering, as apparently exists in GaAs. It is evident that strong intervalley scattering will tend to wipe out the characteristic features of the many-valley solutions mentioned above—different f_0's or T's for different valleys, and $\mathbf{j}$ at an angle to $\mathbf{E}$. This suggests that it would be a better approximation for this case to assume the distribution to be the same for each valley, and this is what was done. There is an additional reason for this approximation to be good in the present case. A substantial part of the carrier heating in the upper valleys, as will be seen, is due to transfer of hot electrons from the (0,0,0) valley, for which the distribution over most of the range of fields is expected to be essentially spherically symmetric. (Even if this were not so the asymmetry would

[40] This equation was obtained earlier for the case $T\gg\Theta$, the Debye temperature, by Dykman and Tomchuk, Ref. 18 and D. Matz, Ref. 17. It was obtained earlier for the parabolic case by R. Stratton, Proc. Roy. Soc. (London) A246, 406 (1958).

[41] See, for example, H. G. Reik and H. Risken, Phys. Rev. 124, 777 (1961).

[42] H. G. Reik and H. Risken, Ref. 41.

bear no simple relation to that expected in the ⟨100⟩ valleys due to a high field.)

For the reasons discussed in Sec. 5 in connection with the lower-valley distribution, the series (5.1) for the upper valley will be terminated also at $n=1$. This will be a better approximation for the upper valleys since the low mobility means that high fields, greater than 12 kV/cm, are required for carrier heating to occur. The $n=1$ terms for the different valleys cannot be expected to be the same even when all valleys are at the same temperature. Since we are concerned ultimately only with the sums of contributions of all the valleys, however, and most of this anisotropy cancels out, it should be a good approximation to calculate for an "average" valley with spherical constant energy surfaces. In any event, no effects of anisotropy nor dependence of the Gunn effect on orientation have been found experimentally.

As discussed in Sec. 4, the scattering processes that must be considered for the upper valley are the intravalley acoustic, polar optical, and intervalley ones. For large $\varepsilon-\varepsilon_0$, where the relaxation time for polar scattering given by (3.1a) applies, polar scattering is found to be much less important for momentum relaxation than equivalent intervalley scattering.[34] For small $\varepsilon-\varepsilon_0$, $\tau_{p0}\to 0$ as $(\varepsilon-\varepsilon_0)^{1/2}$. As discussed earlier for the lower valley, despite the fact that it is not valid for small $\varepsilon-\varepsilon_0$, incorporation of τ_{po} is useful because it simulates the effect of impurity scattering. For the (0,0,0) valley its effect on μ was seen to be equivalent to that of 5×10^{16} impurities per cm^3. For the ⟨100⟩ valleys, because of the larger mass, τ_{po} is smaller, and for a given impurity concentration τ_I would be larger. Use of τ_{po} here would therefore have the effect of a considerably larger impurity concentration. Since the mobility in the upper valleys is already so small that 5×10^{16} impurities per cm^3 would hardly affect it, it appeared a better approximation to omit τ_{po} altogether in calculating the relaxation time for the ⟨100⟩ valleys.

With the dropping of τ_{po} a relaxation time exists for all ε for the upper valleys. Since the upper valleys are parabolic, at least within the range of energies with which we are concerned here, we may use Eqs. (5.5)–(5.10) developed for the lower valley by setting $\Gamma=x$, $\Gamma'=1$. For the upper valleys, however, we must take into account the fact that ε is being measured from the minimum of the (0,0,0) valley, while $\mathbf{k}$ is conveniently measured from the minimum of the ⟨100⟩ valley in which the electron is located. With this, and the notation f_2 for the spherically symmetric ($n=0$) term in the upper-valley distribution, we obtain the differential equation to be solved for the ⟨100⟩ valleys

$$\frac{2e^2E^2}{3m_2\hbar\omega_l}\frac{1}{(x-x_0)^{1/2}}\frac{d}{dx}\times\{(x-x_0)^{3/3}\tau^{(2)}f_2'\}+\left(\frac{\partial f_2}{\partial t}\right)_c=0, \quad (6.1)$$

where

$$x_0=\varepsilon_{02}/\hbar\omega_l. \quad (6.1a)$$

As discussed above, we take the upper-valley relaxation time to be given by

$$\frac{1}{\tau^{(2)}}=\frac{1}{\tau_a}+\frac{1}{\tau_{2\to1}}+\frac{1}{\tau_{j\to j'}}, \quad (6.2)$$

τ_a being given by (3.5a), $\tau_{2\to1}$ by (4.6), and $\tau_{j\to j'}$ by (4.7).

The collision operator is given by

$$\left(\frac{\partial f_2}{\partial t}\right)_c=\left(\frac{\partial f_2}{\partial t}\right)_a+\left(\frac{\partial f_2}{\partial t}\right)_{po}+\left(\frac{\partial f_2}{\partial t}\right)_{2\rightleftarrows1}+\left(\frac{\partial f_2}{\partial t}\right)_{j\rightleftarrows j'}. \quad (6.3)$$

The collision operators for acoustic and polar mode scattering must also be modified to take into account the fact that the bottom of the valleys is at $x=x_0$. This gives for the intravalley acoustic mode scattering

$$\left(\frac{\partial f_2}{\partial t}\right)_a=\frac{4m_2u_l^2}{k_0T}\frac{(2\hbar\omega_l/m_2)^{1/2}(x-x_0)^{1/2}}{l_a}\times\left[\frac{(x-x_0)}{2x_l}f_2''+\left(\frac{x-x_0}{2}+\frac{1}{x_l}\right)f_2'+f_2\right], \quad (6.4)$$

where l_a was defined in (3.5a). Actually $(\partial f_2/\partial t)_a$ was omitted in the final calculations since its effect was found to be very small. The collision operator for the polar scattering is found to be

$$\left(\frac{\partial f_2}{\partial t}\right)_{po}=\frac{2^{1/2}eE_0}{(m_2\hbar\omega_l)^{1/2}}\frac{(x-x_0)^{-1/2}}{e^{x_l}-1}\{\sinh^{-1}(x-x_0)^{1/2}\times[e^{x_l}f_2(x+1)-f_2(x)]+\sinh^{-1}(x-x_0-1)^{1/2}\times[f_2(x-1)-e^{x_l}f_2(x)]\}. \quad (6.5)$$

It is easily verifed that, for $x_0=0$, (6.5) is obtained from (5.11) and (5.12) by replacing $\Gamma(x)$ by x and m_1 by m_2.

From (A20) the collision operator for nonequivalent intervalley scattering is

$$\left(\frac{\partial f_2}{\partial t}\right)_{2\rightleftarrows1}=\left(\frac{m_1}{m_2{}^{(N)}}\right)^{3/2}\frac{1}{\tau_{12}x_0^{1/2}}\{\Gamma^{1/2}(x+x_1)\Gamma'(x+x_1)\times[e^{x_{12}}f_1(x+x_1)-f_2(x)]+\Gamma^{1/2}(x-x_1)\times\Gamma'(x-x_1)[f_1(x-x_1)-e^{x_{12}}f_2(x)]\}, \quad (6.6)$$

where

$$x_1=\omega_{12}/\omega_l, \quad (6.6')$$

$$x_{12}=\hbar\omega_{12}/k_0T, \quad (6.6'')$$

and τ_{12} is defined by (A21). From (A18) and (A19b)

we obtain for the equivalent intervalley scattering

$$\left(\frac{\partial f_2}{\partial t}\right)_{j\rightleftarrows j'}=\frac{1}{\tau_{jj'}x_0^{1/2}}\{(x+x_2-x_0)^{1/2}\times[e^{x_{jj'}}f_2(x+x_2)-f_2(x)]+(x-x_2-x_0)^{1/2}\times[f_2(x-x_2)-e^{x_{jj'}}f_2(x)]\}, \quad (6.7)$$

where, from (A23),

$$x_2=\omega_{jj'}/\omega_l, \quad (6.7')$$

$$x_{jj'}=\hbar\omega_{jj'}/k_0T, \quad (6.7'')$$

and

$$\frac{1}{\tau_{jj'}}=\frac{2}{3}\frac{D_{jj'}{}^2[m_2{}^{(N)}]^{3/2}\varepsilon_{02}{}^{1/2}}{2^{1/2}\pi\hbar^3\rho\omega_{jj'}}\frac{1}{e^{x_{jj'}}-1}, \quad (6.7''')$$

the various symbols here having been defined in Sec. 4. The factor $\frac{2}{3}$ appears in (6.7), as in (4.7), because transitions to the valley at the opposite end of the same cube axis do not require a phonon.

For the (0,0,0) valley the differential equation (5.10) remains valid, but $\tau^{(1)}$ and $(\partial f_1/\partial t)_c$ must be modified to include intervalley scattering. The former is now given by

$$\frac{1}{\tau^{(1)}}=\frac{1}{\tau_{po}}+\frac{1}{\tau_{1\to 2}}, \quad (6.8)$$

where from (A21), (A23), and (A19b),

$$\frac{1}{\tau_{1\to 2}}=\frac{1}{\tau_{12}x_0^{1/2}}[(x+x_1-x_0)^{1/2}+e^{x_{12}}(x-x_1-x_0)^{1/2}]. \quad (6.9)$$

Similarly,

$$\left(\frac{\partial f_1}{\partial t}\right)_c=\left(\frac{\partial f_1}{\partial t}\right)_{po}+\left(\frac{\partial f_1}{\partial t}\right)_{1\rightleftarrows 2}, \quad (6.10)$$

where, from (A22),

$$\left(\frac{\partial f_1}{\partial t}\right)_{1\rightleftarrows 2}=\frac{1}{\tau_{12}x_0^{1/2}}\{(x+x_1-x_0)^{1/2}\times[e^{x_{12}}f_2(x+x_1)-f_1(x)]+(x-x_1-x_0)^{1/2}\times[f_2(x-x_1)-e^{x_{12}}f_1(x)]\}. \quad (6.11)$$

As noted in the Appendix, this is unaffected by the nonparabolicity of the central valley.

If it is desired to include space-charge scattering, $1/\tau_s$, with τ_s given by (3.8), is added to the right of (6.8). The collision operator is unaffected, since this scattering is elastic.

To summarize the discussion carried out so far in this section, the distribution functions f_1 and f_2 for $x>9.2$, i.e., for the energy range in which intervalley scattering is possible, are to be determined by solving a pair of coupled equations. One of these equations is (5.10) with $\tau^{(1)}$ given by (6.8), (A13), and (6.9) and the collision operator by (6.10), (5.11), (5.12), and (6.11). The other equation is (6.1) with $\tau^{(2)}$ given by (6.2), (3.5a), (4.6), and (4.7) and the collision operator by (6.3) through (6.7). The various numerical quantities required are summarized in Table I. In order to make these equations tractable, Taylor-series expansions of $f_i(x\pm x_\alpha)$ were made about the point x and terms of higher order than f_i'' dropped. This leads to difficulty for $x<10$ since $f_2(x)$ is undefined there. It was therefore decided to neglect intervalley scattering in the interval $9.2\leq x\leq 10$. The error that results should be insignificant both because the interval is small and because the density of states in the ⟨100⟩ valley is very small near $x=10$, the valley bottom. The coupled equations are then linear second-order differential equations, and they could be integrated numerically. This again raised the problem of initial values. Integration of the central-valley equation gives $f_1(10)$ and $f_1'(10)$, leaving $f_2(10)$ and $f_2'(10)$ unknown. It was found possible to obtain solutions that were well behaved out to very large values of x for a wide range of values of $f_2(10)$ and $f_2'(10)$. Fortunately, for large x, where various quantities could be expanded, it was possible to carry out a single integration of the differential equation obtained by adding $\Gamma'\Gamma^{1/2}$ times Eq. (5.10) and $(m_2{}^{(N)}/m_1)^{3/2}(x-x_0)^{1/2}$ times Eq. (6.1). This provided a linear relation between f_1, f_1', f_2, and f_2' at large x that could be used in a manner similar to that described earlier for the lower-valley equation to derive a linear relation between f_1, f_1', f_2, and f_2' at $x=10$. Since $f_1(10)$ and $f_1'(10)$ are known, this actually leaves only one unknown parameter, say $f_2(10)$. With the use of the linear relation for large x, plus the condition that f_1 and f_2 must remain positive, it was possible to limit the acceptable $f_1(10)$ values to a very narrow range.

Solutions have been obtained in the manner described for a wide range of fields and different values of the important unknown parameters. One of the most critical has been found to be D_{12}. Since the solutions of the Boltzmann equation describe a steady state, D_{12} affects the distributions mainly through its effect on $\tau^{(1)}$ and thus essentially on how long a time is available for the field to heat the light mass carriers. This effect can be seen in Fig. 4, showing the distributions at a field of 2.4 kV/cm for D_{12} values of 5×10^7 and 5×10^8 eV/cm. In the former case $f_1(x)$ above $x=10$ is a simple continuation of the distribution below $x=10$, while in the latter $f_1(x)$ changes behavior abruptly at $x=10$, dropping so that it becomes essentially parallel to the Maxwell-Boltzmann distribution for $E=0$. As can be seen in Fig. 1, the two cases differ in that for 5×10^7 eV/cm intervalley scattering is ineffective and polar scattering remains dominant above 10, while for 5×10^8 eV/cm intervalley scattering dominates over almost the entire range where it is energetically possible. The intervalley scattering is so strong, in fact, that above 10 the light electrons are no longer heated by the field, as

evidenced by this part of the distribution being parallel to that for $E=0$. So far as f_2 is concerned, it is easily verified that for $E \lesssim E_0$, $\tau^{(2)}$ is too small for any direct heating of the electrons by the field, i.e., the terms involving E in Eq. (6.1) for the upper valleys are negligible. For the larger D_{12} value, where $f_1 \simeq f_2$, the effect of the f_1 terms in (6.1) is also small. Thus, for $E<E_0$, as noted earlier,[3] Eq. (6.1) states essentially, over most of the energy range, $(\partial f_2/\partial t)_c=0$. The solution of this equation, whatever the scattering mechanisms, is, of course, the Maxwell-Boltzmann distribution at the lattice temperature T, as is indeed observed in Fig. 4. For the smaller D_{12}, f_2 just above $x=10$ is not much different from a Maxwellian at temperature T, but as x increases, because f_1 is much larger in this case, the terms in (6.1) become important and f_2 is raised substantially above the lattice temperature Maxwellian, i.e., heating of the carriers in the upper valleys arises from intervalley transfers.

Calculations of the fraction of the electrons in the upper valley, to be discussed in the next section, indicate that for $D_{12}=5\times10^8$ eV/cm 30% of the electrons are in the upper valleys at this field, while for 5×10^7 eV/cm 78% are in the upper valleys. The latter figure is unreasonably high; it would indicate a threshold field for the Gunn effect well below 2.4 kV/cm, which is in contradiction with experimental results. We therefore rejected this value of D_{12} as too low.

Since it has not been established conclusively that low-field avalanche[26] exists, we have carried out the remainder of our calculations for D_{12} values in the range 1 to $5\sqrt{2}\times10^8$ eV/cm. If the low-field avalanche does exist, a D_{12} value near the lower end of this range appears likely,[27] while if it does not exist, a value near the upper end is likely.

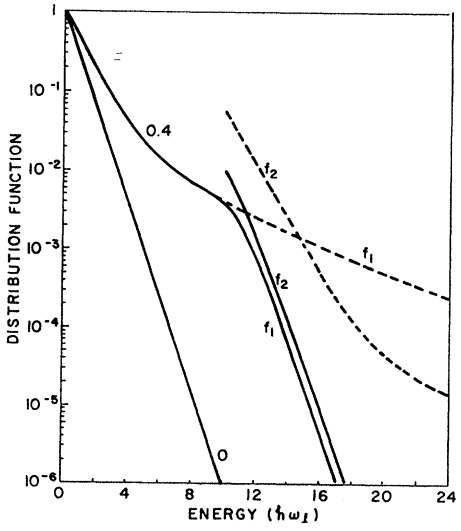

FIG. 4. Distribution functions for electrons in the (0,0,0) and ⟨100⟩ valleys, denoted by f_1 and f_2, respectively, for $E=0.4$ $E_0=2.4$ kV/cm, $D_{jj'}=1\times10^9$ eV/cm, $\alpha=0$ and $D_{12}=5\times10^8$ eV/cm (solid lines) and 5×10^7 eV/cm (dashed lines). The line labeled "0" is the Maxwell-Boltzmann distribution for zero field.

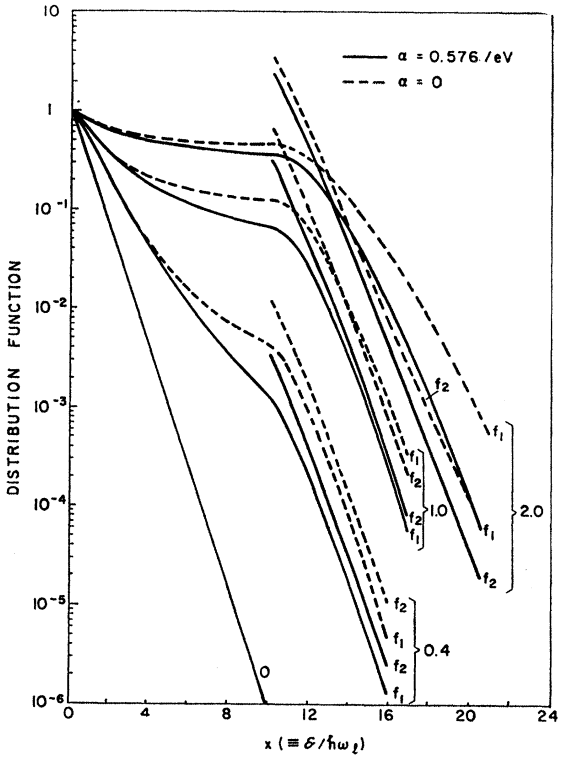

FIG. 5. Distribution functions for electrons in the (0,0,0) and ⟨100⟩ valleys for $E=0.4$, 1.0 and 2.0 E_0, E_0 being 5.95 kV/cm, for parabolic and nonparabolic bands. $D_{12}=5\times10^8$ and $D_{jj'}=1\times10^9$ eV/cm for all plots.

It is implicit in the above discussion that the effect of nonparabolicity is not large. This is shown in Fig. 5, where distributions are plotted for several different fields for $\alpha=0$ and for $\alpha=0.576$/eV or $\alpha\hbar\omega_l=0.02$, the latter, as discussed in Sec. 2, describing the nonparabolicity of GaAs up to 1 eV at least. D_{12} was taken as 5×10^8 eV/cm for all cases. It is seen that for the nonparabolic case the electrons are consistently cooler than for the parabolic. Quantitatively, the same trend exists as was described earlier for $x<10$, e.g., that as the field increases the ratio $f_1^{\rm P}/f_1^{\rm NP}$ at a given x decreases. Not surprisingly, the upper-valley distributions are less affected than the lower ones, the values of $f_2^{\rm P}$ and $f_2^{\rm NP}$ being generally closer together than those of $f_1^{\rm P}$ and $f_1^{\rm NP}$. So far as the variation with field is concerned, for either the parabolic or the nonparabolic case f_1 and f_2 increase monotonically with E, of course. When the field is not too high, above $x=10$ both remain parallel to the $E=0$ line. When the field gets high enough so that the light mass electrons above $x=10$ are heated, the slope of f_1 changes, it crosses f_2 and lies above it at large x. For $\alpha=0$ the light electrons are sufficiently heated at $E/E_0=1$ for this crossing to occur, while for the nonparabolic case the light electrons are

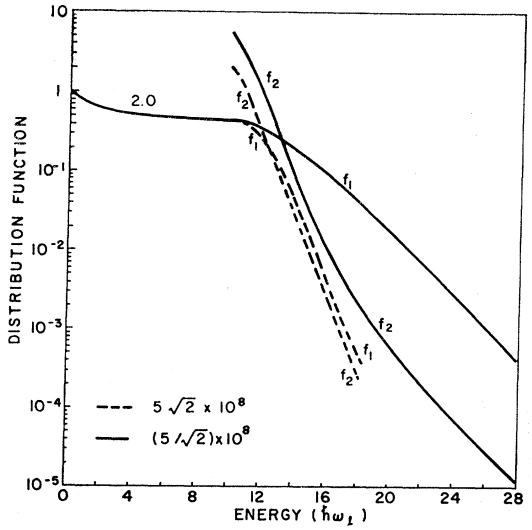

FIG. 6. Distribution functions for electrons in the (0,0,0) and ⟨100⟩ valleys for $E=2.0\ E_0$, E_0 being 5.95 kV/cm, for $\alpha=0$, $D_{jj'}=1\times10^9$ eV/cm and $D_{12}=5\sqrt{2}\times10^8$ eV/cm (dashed lines), $(5/\sqrt{2})\times10^8$ eV/cm (solid lines).

less heated and the crossing does not occur at this field. At $E/E_0=2$ the crossing occurs in both parabolic and nonparabolic cases, although it is clear that the light electrons are more heated in the former case.

Typical high-field behavior is shown more clearly in Fig. 6, which is also designed to illustrate the effect of varying D_{12}. For the smaller D_{12}, where heating of the light mass electrons is greater, f_1 crosses f_2 and stays well above it. f_2 drops rapidly at first and then turns around to become parallel to f_1 at large x, showing the heating of the heavy mass carriers through intervalley transfer referred to earlier. This behavior of f_1 and f_2 is typical of what is seen at higher fields also for this value of D_{12} and at high enough fields for all D_{12}'s investigated, for both parabolic and nonparabolic cases. For the larger D_{12} heating of the light electrons is seen to be much less at this field. Thus even a change by a factor 2 in D_{12} can have a large effect on f_1. The effect on f_2 of this change in D_{12} is considerably less.

Distribution functions at different fields for $D_{12}=1\times10^8$ eV/cm are shown in Fig. 7. As anticipated, f_1 falls off much less rapidly with x for this value of D_{12} than for 5×10^8 eV/cm. At $E/E_0=1$, or 6 kV/cm, f_1 is down by only a factor 10^5 at $x=44$, corresponding to 1.6 eV, the energy required to create an electron-hole pair. It is not unreasonable, therefore, that for this value of D_{12} avalanche could be sustained at 6 kV/cm or somewhat lower, as suggested by Copeland.[26] Apart from the very long tails to high energy, the general behavior of these curves is qualitatively similar to that observed for the other cases. Substantial heating of the light electrons above $x=10$ occurs at lower fields here than for most of the other cases shown because of the smaller D_{12}.

We have investigated also the effects of varying E_0 and $D_{jj'}$. Increases in E_0, predictably, increased the field required to heat the light mass electrons for $x>10$, or, alternatively, decreased this heating at a given field, the general shapes of the distributions being similar to those already shown. The effect of decreasing $D_{jj'}$, or the rate of equivalent intervalley scattering, is shown in Fig. 8 for a field of 36 kV/cm. Very high fields are required for this effect to be sizable. For fields up to 12 kV/cm the effect of changing $D_{jj'}$ by as much as a factor 2 is quite small since the upper-valley mobility remains small and carrier heating above $x=10$ is small for the parameters used here. It is seen that decreasing $D_{jj'}$ raises both f_1 and f_2, presumably because the higher mobility of the heavy mass carriers permits more direct heating by the field. For $D_{jj'}=5\times10^8$ eV/cm the closeness of the light and heavy electron disbribution functions is a consequence of their mobilities being comparable at this field.

Distribution functions were also obtained for cases in which space-charge scattering was included. Again, the shapes of f_1 and f_2 were similar to those shown above. The main effect of the incorporation of τ_s was that higher fields were required to produce a comparable amount of electron heating.

7. VARIATION WITH FIELD OF $n_1/(n_1+n_2)$, v_d, μ, μ_2, ETC.

The functions f_1 and f_2 obtained from the numerical calculations described are unnormalized. The normalized functions may be taken as $\mathcal{C}f_1$ and $\mathcal{C}f_2$, the normalization factor being the same for both since the differential equations are coupled. To determine $\mathcal{C}$ we use

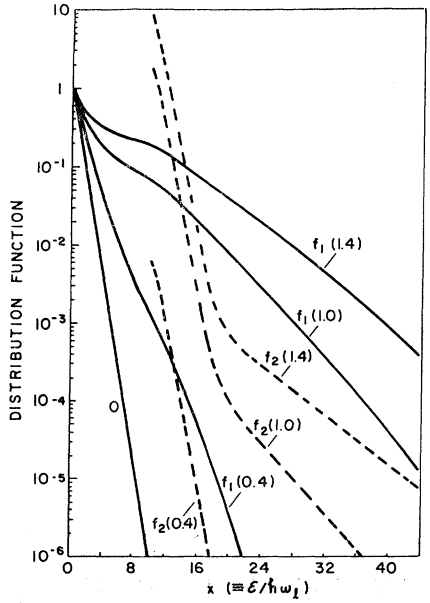

FIG. 7. Distribution functions for electrons in (0,0,0) and ⟨100⟩ valleys for $E=0.4$, 1.0, and 1.4 E_0, E_0 being 5.95 kV/cm, for a nonparabolic band with $D_{12}=1\times10^8$ eV/cm, $D_{jj'}=1\times10^9$ eV/cm.

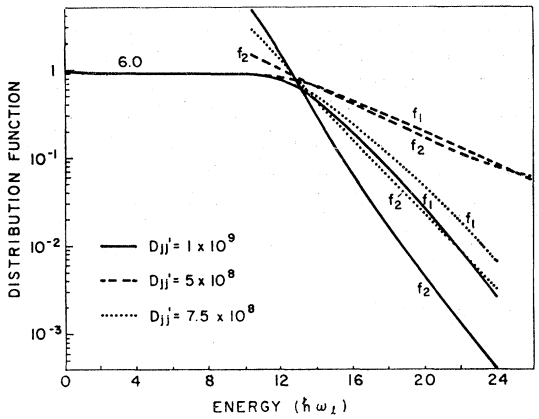

FIG. 8. Distribution function for electrons in the (0,0,0) and ⟨100⟩ valleys for $E=6.0\ E_0$, E_0 being 6.31 kV/cm, $\alpha=0$, $D_{12}=5\sqrt{2}\times10^8$ eV/cm and $D_{jj'}$ values of 5×10^8 eV/cm (dashed lines), 7.5×10^8 eV/cm (dotted lines) and 1×10^9 eV/cm (solid lines)

the condition that the total carrier concentration n_T is given by

$$n_T=n_1+n_2=\sum_{\mathbf{k}^{(1)}} f_1+\sum_{\mathbf{k}^{(2)}} f_2, \tag{7.1}$$

where the first summation is to be taken over all states in the (0,0,0) valley, the second over all states in the ⟨100⟩ valleys. Carrying out these summations, taking into account the nonparabolicity of the central valley, we obtain

$$n_T=8\pi 2^{1/2}m_1^{3/2}(\hbar\omega_l)^{3/2}\mathfrak{A}[\mathcal{J}_1+\mathcal{J}_2]/h^3, \tag{7.2}$$

where

$$\mathcal{J}_1=\int_0^\infty \Gamma^{1/2}(x)\Gamma'(x)f_1 dx \tag{7.3}$$

and

$$\mathcal{J}_2=(m_2^{(N)}/m_1)^{3/2}\int_{x_0}^\infty (x-x_0)^{1/2}f_2 dx. \tag{7.4}$$

It is clear that the first term of (7.3) corresponds to n_1, the second to n_2. We therefore deduce

$$n_1/(n_1+n_2)=\mathcal{J}_1/(\mathcal{J}_1+\mathcal{J}_2). \tag{7.5}$$

Since we have taken the distributions in the form $f^{(i)}=f_i+k_E g_i$, we may write the current density

$$\mathbf{j}=e[\sum_{\mathbf{k}^{(1)}} \mathbf{v}k_E g_1+\sum_{\mathbf{k}^{(2)}} \mathbf{v}k_E g_2], \tag{7.6}$$

where again the first summation is over all states in (0,0,0), the second over all states in the ⟨100⟩ valleys. For spherical constant energy surfaces only the component of $\mathbf{v}$ along $\mathbf{E}$ will contribute to the current. In a nonparabolic band a component of $\mathbf{v}$, v_α, is related to the corresponding component of $\mathbf{k}$, k_α, by

$$v_\alpha=\hbar k_\alpha/m_1(d\gamma/d\varepsilon). \tag{7.7}$$

Using (7.7) and (5.9), and replacing k_E^2 by its average over a constant energy surface, $2m_1\gamma/3\hbar^2$ for (0,0,0) and $2m_2(\varepsilon-\varepsilon_{02})/3\hbar^2$ for ⟨100⟩, we obtain

$$j=-\tfrac{2}{3}e^2E\left[\sum_{\mathbf{k}^{(1)}}\frac{\gamma\tau^{(1)}}{m_1(d\gamma/d\varepsilon)^2}\frac{df_1}{d\varepsilon}+\sum_{\mathbf{k}^{(2)}}\frac{(\varepsilon-\varepsilon_{02})\tau^{(2)}}{m_2}\frac{df_2}{d\varepsilon}\right]. \tag{7.8}$$

Changing the summations to integrations with use of (A19a) and (A19b) for the densities of states, and incorporating the value of $\mathfrak{A}$ obtained from (7.2), we find finally

$$j=n_T e v_d=-\frac{2}{3}\frac{n_T e^2\tau_{12}E}{m_1(\mathcal{J}_1+\mathcal{J}_2)}(\mathcal{J}_1+\mathcal{J}_2), \tag{7.9}$$

where

$$\mathcal{J}_1=\int_0^\infty \frac{\Gamma^{3/2}(x)}{\Gamma'(x)}\frac{\tau^{(1)}}{\tau_{12}}f_1' dx \tag{7.10}$$

and

$$\mathcal{J}_2=g_j\left(\frac{m_2}{m_1}\right)^{1/2}\int_{x_0}^\infty (x-x_0)^{3/2}\frac{\tau^{(2)}}{\tau_{12}}f_2' dx, \tag{7.11}$$

g_j being the number of equivalent ⟨100⟩ valleys. The first term of (7.9) represents the current contribution of the (0,0,0) valley and the second that of the ⟨100⟩ valleys. The drift velocity calculated from (7.9) represents, of course, an average over the two sets of valleys. By combining (7.9) and (7.5) we may deduce the mobility of electrons in the (0,0,0) valley:

$$\mu_1=-\frac{2e\tau_{12}}{3m_1}\frac{\mathcal{J}_1}{\mathcal{J}_1}. \tag{7.12}$$

Similarly, we may deduce the mobility of electrons in the ⟨100⟩ valleys:

$$\mu_2=-\frac{2e\tau_{12}}{3m_1}\frac{\mathcal{J}_2}{\mathcal{J}_2}. \tag{7.13}$$

For calculations of domain dynamics it is necessary to know also the diffusion constant D of the carriers. By solving the Boltzmann equation under the usual assumption that the distribution function varies little over a mean free path, one finds[43]

$$D=\tfrac{1}{3}\langle\tau v^2\rangle. \tag{7.14}$$

This should be valid for diffusion perpendicular to the current direction, approximately so for diffusion along the current direction.[44] With the use of (7.7) we find for a nonparabolic band

$$D=\frac{2}{3m_1}\left\langle\frac{\tau\gamma}{(d\gamma/d\varepsilon)^2}\right\rangle. \tag{7.15}$$

Inserting the density of states (A19a), we obtain from

[43] See, for example, E. M. Conwell, Phys. Rev. **127**, 1493 (1962).
[44] P. J. Price, in *Fluctuations in Solids*, edited by R. E. Burgess (Academic Press Inc., New York, 1965), Chap. 8.

(7.15)

$$D_1=\frac{2\hbar\omega_l\tau_{12}}{3m_1\mathcal{G}_1}\int_0^\infty\frac{\Gamma^{3/2}(x)}{\Gamma'(x)}\frac{\tau^{(1)}}{\tau_{12}}f_1\,dx. \quad (7.16)$$

Comparison of (7.16) with (7.12), using (7.10) for $\mathcal{G}_1$, shows that if f_1 were a Maxwell-Boltzmann distribution the Einstein relation would be satisfied, as of course it should be. From (7.14) and (A19b) we deduce for the upper-valley electrons

$$D_2=\frac{2\hbar\omega_l\tau_{12}}{3m_2^{(I)}\mathcal{G}_2}\left[\frac{m_2^{(N)}}{m_1}\right]^{3/2}\int_{x_0}^\infty(x-x_0)^{3/2}\frac{\tau^{(2)}}{\tau_{12}}f_2\,dx, \quad (7.17)$$

where $m_2^{(I)}$ is the inertial mass of the upper-valley electrons.[43] In this case the Einstein relation should be reasonably well satisfied over much of the field range of interest because the upper-valley distribution is close to Maxwellian. It is also useful to calculate an average diffusion constant, $\bar{D}$, for the two types of carrier, defined by

$$\bar{D}=\frac{n_1}{n_1+n_2}D_1+\frac{n_2}{n_1+n_2}D_2. \quad (7.18)$$

Another quantity of interest is the average energy of the carriers. For the lower-valley electrons this is given by

$$\langle\varepsilon_1\rangle=(\hbar\omega_l/\mathcal{G}_1)\int_0^\infty\Gamma^{1/2}(x)\Gamma'(x)xf_1\,dx, \quad (7.19)$$

while for the upper valley

$$\langle\varepsilon_2\rangle=(\hbar\omega_l/\mathcal{G}_2)[m_2^{(N)}/m_1]^{3/2}\int_{x_0}^\infty(x-x_0)^{3/2}f_2dx. \quad (7.20)$$

The integrals $\mathcal{J}_1$, $\mathcal{J}_2$, $\mathcal{G}_1$, $\mathcal{G}_2$, and those of Eqs. (7.16), (7.17), (7.19), and (7.20) were evaluated numerically. Some results for the average drift velocity versus field are shown in Figs. 9–11. Figure 9 shows the effect of including nonparabolicity in the calculations. As expected from the fact that this caused the distribution to be cooler, the beginning of the negative differential resistance (ndr) region or threshold comes at a higher field in the nonparabolic case, 2.9 kV/cm, as compared with 2.1 kV/cm, D_{12} being 5×10^8 eV/cm in both cases. Correspondingly, for this value of D_{12} the minimum is at 12 kV/cm in the nonparabolic case as compared with 10 kV/cm in the parabolic case. The differential mobility in the negative differential resistance region is quite similar in the two cases, about -3000 cm^2/V sec in the steeper region of the characteristic. For $D_{12}=1\times10^8$ eV/cm the threshold is lower, about 2.4 kV/cm,

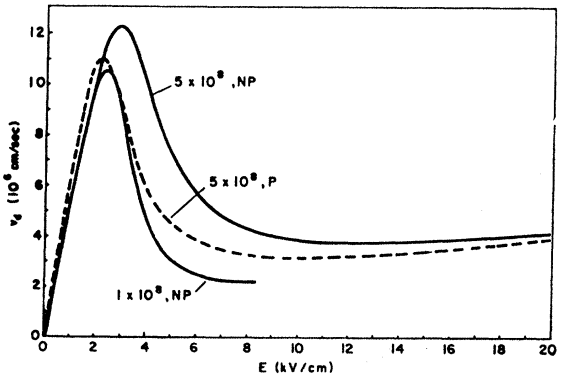

FIG. 9. Average drift velocity versus field for $D_{12}=5\times10^8$ eV/cm for both parabolic and nonparabolic bands and for $D_{12}=1\times10^8$ eV/cm for the nonparabolic band. For all plots $E_0=5.95$ kV/cm and $D_{jj'}=1\times10^9$ eV/cm.

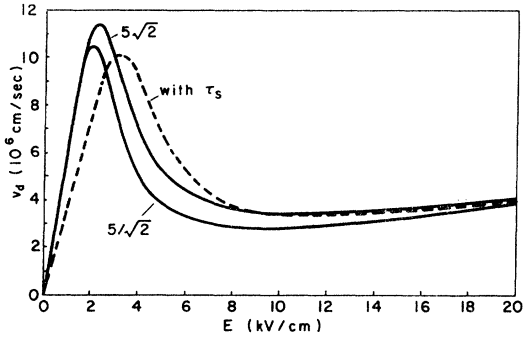

FIG. 10. Average drift velocity versus field for D_{12} values of $(5/\sqrt{2})$ and $5\sqrt{2}\times10^8$ eV/cm, and for $D_{12}=5\times10^8$ eV/cm with space-charge scattering as described in the text. For all plots $E_0=5.95$ kV/cm, $D_{jj'}=1\times10^9$ eV/cm, and $\alpha=0$.

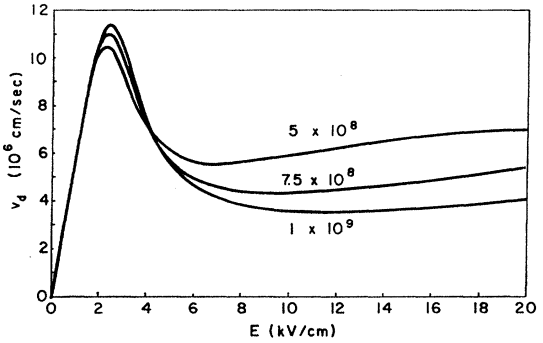

FIG. 11. Average drift velocity versus field for $D_{jj'}$ values of 1×10^9, 7.5×10^8, and 5×10^8 eV/cm. For all plots $D_{12}=5\sqrt{2}\times10^8$ eV/cm, $E_0=6.31$ kV/cm, and $\alpha=0$.

as expected because the smaller D_{12} permits the electrons to get hotter. For the same reason the drift velocity comes down more steeply beyond threshold for this D_{12}. The effect of varying D_{12} is also shown in the next figure, where it is seen that for $D_{12}=5\sqrt{2}\times10^8$ eV/cm the threshold is at 2.2 kV/cm, while for $(5/\sqrt{2})\times10^8$ eV/cm it is at 2.0 kV/cm. This figure shows also the effect on the characteristic of space-charge scattering, to the crude approximation employed here. For the latter calculations N_sQ was taken to be 3.2×10^4 cm^{-1}, which, when the other scattering processes are included, leads to a low-field mobility of 5500 cm^2/V sec for a

sample with 10^{15} impurities per cm^3. Incorporation of this amount of space-charge scattering raises the threshold from 2.1 kV/cm to 3.3 kV/cm and the minimum or valley from 10 to 12 kV/cm. It also decreases the magnitude of the differential mobility in the ndr region somewhat. In Fig. 11 we show the effect of varying $D_{jj'}$. When $D_{jj'}$ is decreased μ in the upper valleys increases, with the consequence, shown in Fig. 8, that both (0,0,0)- and ⟨100⟩-valley electrons are heated more. This leads to the threshold and valley fields decreasing as $D_{jj'}$ decreases, the former effect being relatively small, however, because heating of the upper-valley electrons is small for any of these $D_{jj'}$ values at fields around threshold. The fact that current is higher beyond the minimum for the lower $D_{jj'}$ is, of course, due to μ_2 being higher. For $D_{jj'}=5\times10^8$ eV/cm, in fact, μ_2 is high enough to allow perceptible electron heating and consequent decrease of mobility at the highest fields shown, as evidenced by the flattening of the characteristic there. This is shown more directly in Fig. 12 where μ_2 is plotted versus field for various different values of the parameters. It is clear, as indicated earlier, that μ_2 is quite sensitive to the value of $D_{jj'}$, 1×10^9 eV/cm giving the value in best agreement with experiment. Changing the value of the deformation potential from 6 to $6\sqrt{2}$ eV has relatively little effect on μ_2 because the deformation potential scattering is relatively unimportant.

It is noteworthy that changes in D_{12} have little effect on μ_2 even when the effect on f_2 is considerable, as in the case shown in Fig. 6, for example. The reason for this is that, since $\tau^{(2)}$ decreases as x increases, the part of the distribution that makes the greatest contribution to μ_2 is that in the neighborhood of $x=10$. Thus any heating at large x has little effect on μ_2. In the neighborhood of $x=10$ the main effect on f_2 of change in D_{12}, shown in Fig. 6, is a shift with little change in slope. Since μ_2 is determined essentially by f_2' rather than f_2 such a shift causes little change.

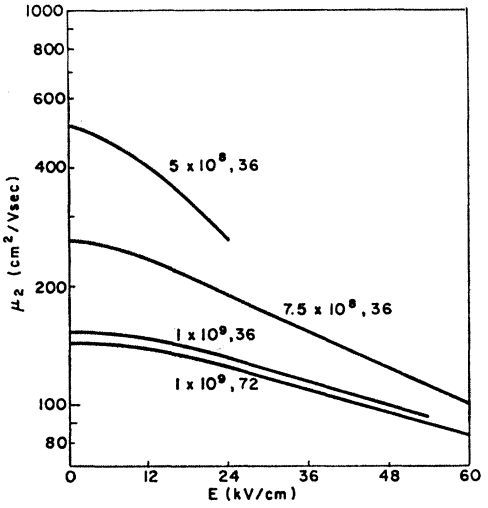

FIG. 12. Mobility versus field for carriers in the ⟨100⟩ valleys for $D_{jj'}$ values of 5×10^8, 7.5×10^8, and 1×10^9 eV/cm and E_1^2 values of 36 and 72 eV. For all plots $D_{12}=5\sqrt{2}\times10^8$ eV/cm, $E_0=6.31$ kV/cm, and $\alpha=0$.

The variation of the (0,0,0)-valley mobility with D_{12} and field is shown in Fig. 13. For fields below threshold μ_1 shows a slight increase with field, this being only about 4%, for example, for the nonparabolic case with $D_{12}=5\times10^8$ eV/cm. This increase might be due to the (simulated) impurity scattering. Inclusion of space-charge scattering would make the increase smaller or cause μ_1 to decrease, depending on the amount of this scattering included. Measurements below threshold on samples with $n\simeq4\times10^{15}$/cm^3, lower than the impurity concentration for which we calculate, in effect, gave a Hall mobility that decreased somewhat with increasing field.[45] The mobility, ~7000 cm^2/V sec, was lower than the theoretical mobility including impurity scattering for such samples, >8000 cm^2/V sec, suggesting the presence of space-charge scattering. It may therefore

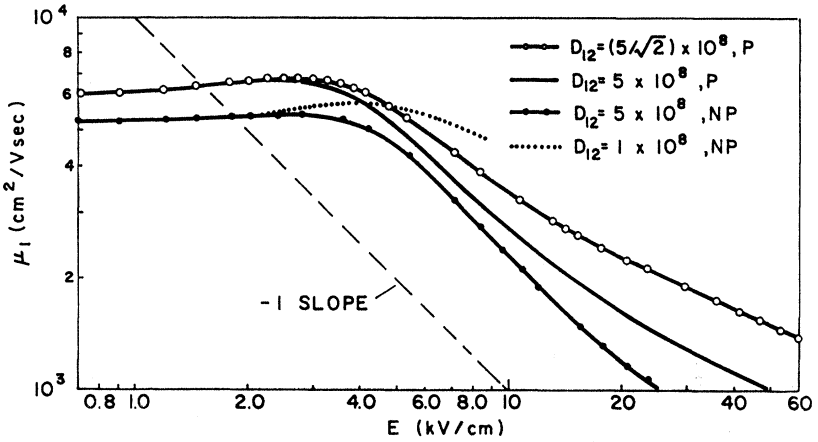

FIG. 13. Mobility versus field for carriers in the (0,0,0) valley for the D_{12} values specified. For all plots $E_0=5.95$ kV/cm, $D_{jj'}=1\times10^9$ eV/cm. The dashed line shows a -1 slope for comparison.

[45] A. Zylbersztejn and J. B. Gunn, Phys. Rev. **157**, 668 (1967).

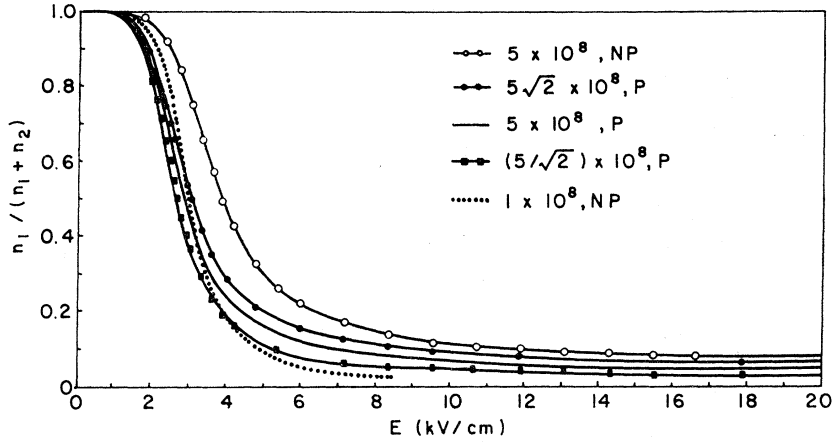

FIG. 14. Fraction of carriers in the (0,0,0) valley as a function of field for the D_{12} values specified. For all plots $E_0=5.95$ kV/cm and $D_{jj'}=1\times10^9$ eV/cm.

be the case that the drift mobility, which is what we calculate, and Hall mobility vary in the same way with field although, of course, in principle they need not. Since in any case the calculations need not be accurate in this range of fields we can only conclude that changes in μ_1 below threshold are small. Beyond threshold μ_1 decreases with increasing E due to the influence of intervalley scattering, the more rapidly the larger D_{12}. It is seen from the plot that for the cases of stronger intervalley scattering, or larger D_{12}, μ_1 shows a region of -1 slope, or drift velocity independent of field. It is interesting to note that this occurs in about the same field range for which drift velocity is found to be independent of field in Ge at room temperature. An explanation has been presented for this so-called saturation in Ge in terms of a combination of intravalley deformation potential and nonpolar optical scattering.[46] This explanation has been challenged, however, on the grounds that it neglects intervalley scattering, which must have a considerable effect in this field range.[47,48] We note also

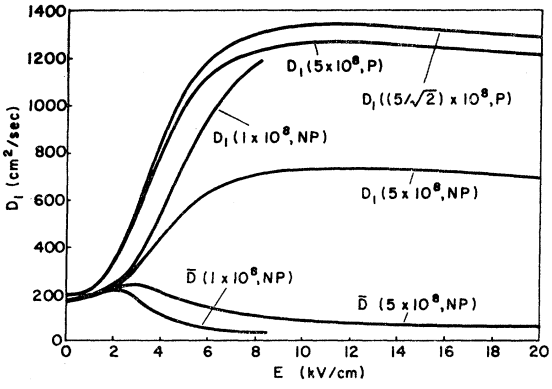

FIG. 15. Variation with field of diffusion constant D_1 for the (0,0,0) carriers and of average diffusion constant $\bar{D}$ for the D_{12} values shown. For all plots $E_0=5.95$ kV/cm and $D_{jj'}=1\times10^9$ eV/cm.

that D_{12} for scattering between the lower valleys [$\langle111\rangle$ in Ge] and upper valleys [also $\langle100\rangle$ in Ge] is 5×10^8 eV/cm.[49]

The variation with field of the valley populations is shown in Fig. 14, where n_1/n_T is plotted versus field. It is seen that once the transfer of carriers has begun, a little below threshold, it proceeds very rapidly. At the threshold about 20% of the carriers have transferred to the upper valleys. The fact that the transfer is larger at a given field the smaller D_{12} is again a consequence of the greater carrier heating for smaller D_{12}.

The results of Fig. 14 for low fields may be compared with the data of Zylbersztejn and Gunn mentioned above. From their experiments[45] they concluded that the fractional change in n_1 at a field of 2 kV/cm was small, less than $\sim2\%$. For the parabolic case this change, according to Fig. 14, is 14 to 20%. For the nonparabolic case, however, the change at 3 kV/cm is 5%. With space-charge scattering taken into account the calculated change would be less than 5%. Thus the results with nonparabolicity taken into account are in good agreement with these experimental data.

Figure 15 shows the variation with field of the diffusion constant for the (0,0,0) carriers and of the average diffusion constant. The diffusion constant for the $\langle100\rangle$ carriers is not shown, because it stayed almost constant through the field range shown, as expected. For low fields D_1 for the case $\alpha=0$ is 206 cm²/sec, whereas the value calculated from the Einstein relation is 160 cm²/sec. The poor agreement is not unexpected since, as noted earlier, the approximations made are not particularly good at low fields. The initial increase in D_1 with increasing E reflects the rapid increase in $\langle\varepsilon\rangle$ with field, shown in Fig. 16, which more than counterbalances the decrease in τ with E due to increasing mass and inter-

[46] H. G. Reik and H. Risken, Phys. Rev. **126**, 1737 (1962).
[47] E. G. S. Paige, in *Progress in Semiconductors*, edited by A. F. Gibson and R. E. Burgess (John Wiley & Sons, Inc., New York, 1964), Vol. 8.
[48] N. I. Meyer and M. H. Jorgensen, J. Phys. Chem. Solids **26**, 823 (1965).
[49] S. M. de Veer and H. J. G. Meyer, in *Proceedings of the International Conference on Physics of Semiconductors, Exeter, 1962*, edited by A. C. Stickland (Institute of Physics and The Physical Society, London, 1962), p. 358.

valley scattering. For the upper valleys the Einstein relation is expected to hold quite well over most of the field range shown because the distribution is essentially Maxwellian. The calculated D_2, with m_2 taken as the value in Table I, was 4.8 cm²/sec, while the value obtained from the Einstein relation with $\mu=150$ cm²/V sec was 3.7 cm²/sec. In this case the discrepancy arises from the fact that the masses have not been handled correctly, i.e., the many-valley model has not been used consistently. In calculating $\bar{D}$ therefore we used for D_2 the value obtained from the Einstein relation. It is seen in Fig. 15 that starting from threshold the upper-valley carriers dominate $\bar{D}$, the value being lower for $D_{12}=1\times10^8$ than for 5×10^8 eV/cm because more carriers are in the upper valley at a given field for the former value.

The variation with field in average energy of the (0,0,0) carriers is shown in Fig. 16. As remarked earlier, the initial increase is fairly rapid. An $\langle\varepsilon\rangle$ of $4\hbar\omega_l$, where the approximations of the present calculations should begin to be good, is attained by about 4 kV/cm. At the lower fields the nonparabolic case lies below the parabolic for the same D_{12}, but the difference becomes very small at higher fields, as expected from the small differences in the distribution functions there. In all cases but that of $D_{12}=1\times10^8$ eV/cm the rate of increase is not as rapid at the higher fields because of the greater influence of intervalley scattering. For the upper valleys the energy does not begin to increase until fields well above threshold are reached and then increases only slowly. At 20 kV/cm the increase in the average energy of the upper-valley electrons is only about 25%.

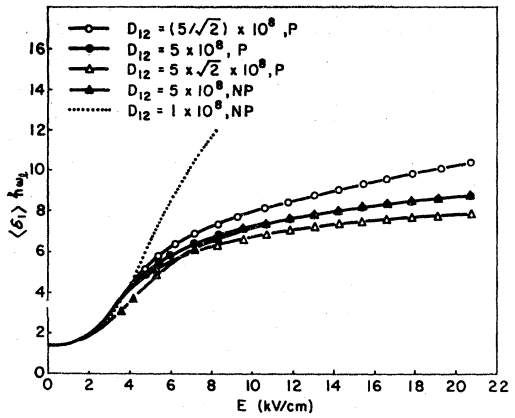

FIG. 16. Variation with field of average energy, measured in units of $\hbar\omega_l$, of the (0,0,0) carriers for the D_{12} values shown. For all plots $E_0=5.95$ kV/cm and $D_{jj'}=1\times10^9$ eV/cm.

8. DISCUSSION OF RESULTS AND COMPARISON WITH EXPERIMENT

The principal approximations made in the present calculations are: (1) choice of the (0,0,0) valley distribution in the form (5.2), i.e., the assumption that the distribution is approximately isotropic, and (2) keeping only terms quadratic in $\hbar\omega/\varepsilon$ in expansions of quantities such as $f(\varepsilon\pm\hbar\omega)$. Stenflo[39] has contended that the first approximation is responsible for the difference between our calculations and the experimental results, which at that time consisted of the Gunn and Elliott[50] measurement of v_d versus E. This was his motivation, in fact, for carrying out the calculations using the maximum anisotropy distribution referred to in Sec. 5. Using the same parameters as we have, with $D_{12}=5\times10^8$ eV/cm, and neglecting nonparabolicity, Stenflo found that at 2.4 kV/cm the fraction of electrons in the upper valleys according to the maximum anisotropy calculation would be 60%, as compared with 30% for calculations he did using our approximation, which he calls the diffusion approximation. The latter value agrees fairly well with our results, as can be seen in Fig. 14. The 60% would correspond to a threshold well below 2.4 kV/ cm.

[50] J. B. Gunn and B. J. Elliott, Phys. Letters **22**, 369 (1966).

The fact that the maximum anisotropy distribution gives more carriers in the upper valley at a given field would appear to result from the enforced streaming of the carriers causing them to be hotter. Stenflo has also done the maximum-anisotropy calculations including nonparabolicity for the central valley. For this purpose he assumed

$$\frac{1}{\hbar}\frac{d\varepsilon}{dk}=\left(\frac{2\varepsilon_1}{m_1}\right)^{1/2}\sin\left(\frac{\varepsilon}{\varepsilon_1}\right)^{1/2}, \tag{8.1}$$

where ε_1 is a parameter. The calculations were carried out for ε_1 values of 4θ and 10θ, θ being 418°K. For small $\varepsilon/\varepsilon_1$ the relation (8.1) is similar to what would be obtained by differentiating (2.4). To obtain correspondence with GaAs an ε_1 value lying between 4θ and 10θ would be required. With this nonparabolicity, Stenflo obtains the results that for 2.4 kV/cm the fraction of carriers in the upper valleys is 30% for $\varepsilon_1=4\theta$, 50% for $\varepsilon_1=10\theta$. Thus the calculated threshold with this approximation would lie below 2.4 kV/cm even with nonparabolicity included. Although the experimental values scatter greatly, as will be seen, the preponderance of evidence is for a threshold above 2.4 kV/cm. Thus the assumption of an approximately isotropic distribution would seem to be the better one over all. It should, in any event, be reasonably good at fields past about 4 kV/cm, where $\langle\varepsilon\rangle>4\ \hbar\omega_l$.

An approximation quite different from ours has been made by Butcher and Fawcett, who assumed that $f_1(\varepsilon)$ and $f_2(\varepsilon)$ are displaced Maxwellians. In their original calculations,[51] Butcher and Fawcett took into account only polar and nonequivalent intervalley scattering. This resulted in a predicted threshold field of 3.2 kV/cm and a minimum of 5.8 kV/cm followed by a fairly rapid rise in v_d. Since these latter two results were in obvious disagreement with experiment, they[52] repeated their

[51] P. N. Butcher and W. Fawcett, Proc. Phys. Soc. (London) **86**, 1205 (1965).

[52] P. N. Butcher and W. Fawcett, Phys. Letters **21**, 489 (1966).

calculations taking into account for the upper valleys intravalley acoustic scattering with $E_1=7$ eV and equivalent intervalley scattering with $D_{jj'}=1\times10^9$ eV/cm. The other numerical values used were quite similar to those assumed here, with $D_{12}=6\times10^8$ eV/cm. In the new results the threshold remained at 3.2 kV/cm, but the minimum moved out to 25 kV/cm. Nonparabolicity was not included in their calculations. As compared with our own calculations for $D_{12}=5\times10^8$ eV/cm omitting nonparabolicity, both threshold and minimum are much higher. This was to be expected from the fact that the correct distribution has relatively more high-energy carriers and fewer low-energy carriers than permitted by the Maxwellian form of the same $\langle\varepsilon\rangle$.

The effect of the second approximation, that of replacing quantities such as $f(\varepsilon\pm\hbar\omega)$ by Taylor-series expansions carried out to terms quadratic in $\hbar\omega/\varepsilon$, is less clear. One would guess that it amounts to assuming that the scattering is more elastic than it really is. The consequence of this would be increased heating of the carriers, thus a lowered threshold. In any event, this effect, like the first discussed, should no longer be significant at fields for which the scattering is reasonably elastic, i.e., past about 4 kV/cm.

So far as the physical model used is concerned, the main question is the location of the $\langle111\rangle$ valleys. If these valleys are 0.45 to 0.5 eV above the conduction-band minimum, corresponding to $x=12.5$ to 14, and the $1.2m_0$ includes most of their contribution to the density of states, as speculated earlier, then the present calculations have to a fair approximation taken their effect into account. We may speculate further that, correctly incorporated, they would not have much effect on the location of the minimum but would have the effect of raising the v_d versus E curve past threshold, decreasing the peak-to-valley ratio. The latter effect would occur because the mobility in the $\langle111\rangle$ valleys is expected to be higher because of the smaller mass. Some examples of the effect of higher mobility in the upper valleys were shown in Fig. 11. The effect of electrons populating the $\langle111\rangle$ minima is not expected to be large, however, because less than half the electrons would be in these minima in any case and there is no reason to expect their mobility to be very much higher than that in the X_1 minima.

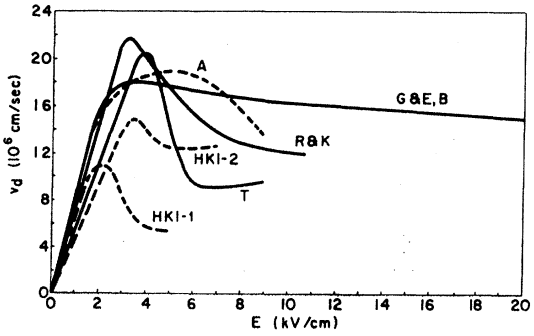

FIG. 17. Experimental drift velocity versus field determinations of Gunn and Elliott (G and E) (Ref. 50); Thim (T) (Ref. 53); Ruch and Kino (R and K) (Ref. 54); Acket (A) (Ref. 55); Hamaguchi, Kono, and Inuishi (HKI) (Ref. 56); and Braslau (B) (Ref. 57).

So far as parameters to be put into the calculation are concerned, the really important missing one is D_{12}. Its effects are clearly not minor, and it must be known in order to get conclusive results. It should be possible to determine it by careful studies of transport in GaAs under sufficient hydrostatic pressure to make the separation between X_1 and Γ_1 small. This technique has the additional advantage of removing the L_1 minima from the vicinity.

It had originally been hoped that measurements of v_d versus E would give an indication of the value of D_{12}. This hope has had to be abandoned, at least for the present. The determination of v_d versus E in the ndr region is not straightforward because of the tendency for the potential drop to be nonuniform there. Nevertheless, a variety of experimental determinations of v_d versus E now exists, with an approximately equal variety of experimental results. These are displayed in Fig. 17.[53–57] The results of Acket and of Hamaguchi, Kono and Inuishi are shown dashed because they did not give their results in the form of drift velocity versus field. Drift velocities have been calculated from their reported results by assuming in the former case that μ_0 for the reported samples was the same as that for the Gunn and Elliott sample, and in the latter case that $n_T=2\times10^{15}/\text{cm}^3$ for sample ME-2, shown here as HKI-2, and $1\times10^{15}/\text{cm}^3$ for sample ME-1, shown here as HKI-1.

With the exception of the R and K sample, which was semi-insulating, and HKI-1, which had a resistivity of 0.5 Ω cm, all the samples measured were in the 1–20-Ω cm range. The measurements of Acket, Hamaguchi *et al.*, and Braslau were done with a microwave technique in which it was presumed that the time the field was in the ndr region was too short for appreciable field inhomogeneities to build up. The same presumption underlay the measurements of Gunn and Elliott, done with very short dc pulses. The measurements of Ruch and Kino and of Thim, on the other hand, were made on samples in which the product of n_T and sample length l was too small to allow domain formation. In the Ruch and Kino case the potential redistribution could be neglected, and v_d was obtained from the time required for an injected pulse of carriers to drift a known distance. Thim used very short semiconducting samples and deduced v_d from measurements of the potential distribution along the sample by means of

[53] H. W. Thim, Electron. Letters **2**, 403 (1966).
[54] J. G. Ruch and G. S. Kino, Appl. Phys. Letters **10**, 40 (1967).
[55] G. A. Acket, Phys. Letters **24A**, 200 (1967).
[56] C. Hamaguchi, T. Kono, and Y. Inuishi, Phys. Letters **24A**, 500 (1967).
[57] N. Braslau, Phys. Letters **24A**, 531 (1967).

Poisson's equation and the current continuity condition. Measurements of Chang and Moll, made also on semi-insulating material, are not shown here. Their published results,[58] taken out to 9.5 kV/cm, had almost exactly the shape of the curve labeled 5×10^8, P in Fig. 9, with a threshold of 2.2 kV/cm. These results were based on the assumption that the trapping time for carriers in their sample was independent of field. It has since been discovered[54] that this trapping time varied with field, decreasing initially. This would have the effect of raising the threshold somewhat,[59] and of course otherwise modifying their curve.

The differences shown in Fig. 17 are not yet explained. Indeed, some may be due to experimental error or limitations, as yet not understood, of the experimental techniques. It is difficult to escape the conclusion, however, that at least some of the differences are due to differences between the samples. For example, the two samples of HKI were measured with the same technique, whatever its limitations, differed in ρ by only 0.5 Ω cm, and yet have thresholds of 2.1 kV/cm and 3.4 kV/cm, respectively, and quite different characteristics. Braslau's determination, made by precisely the same technique as HKI and Acket, on a sample from the same crystal as the G and E sample, gave results essentially identical with those of G and E. Yet these results give a much lower differential mobility, -300 cm^2/V sec, than obtained in any of the other v_d versus E determinations. A determination of differential mobility by McWhorter and Foyt[60] from a study of negative conductance amplification gave a value in the range -2500 to -3000 cm^2/V sec, more or less in agreement with most of the other experimental determinations and the theoretical calculations.

It has been suggested by Copeland and others that the differences between the G and E results and others might be due to generation of carriers in their samples by impact ionization of the lattice.[61] In fact, according to the published α versus E,[26] all samples investigated should have shown carrier multiplication above about 5 kV/cm. It has been demonstrated, however, that there was no increase in carrier concentration in the G and E sample.[62] The only determinations in which any impact ionization was observed are those of Thim[53] and HKI-1.[63] It was not determined in these cases whether the ionization was that of impurities or of the lattice. It is significant that these two determinations show the steepest decrease of v_d with E beyond threshold, indicating the greatest heating of the carriers. We shall return to the discussion of this point later on.

So far as agreement with our theory is concerned, the experimental thresholds are all high except for those of HKI-1 and R and K. A threshold matching the latter, 3.2 kV/cm, could be obtained by increasing D_{12} to $\sim8\times10^8$ eV/cm. The thresholds found by G and E, Thim and Acket, are 3.6–3.8, 3.9, and 5 kV/cm, respectively. Drift velocity at threshold is higher for the experimental curves, except for HKI-1, but this is not particularly significant. Partly this is due to the fact that μ_0 of the experimental samples was substantially higher than μ_0 used in the calculations, which was 5 to 6×10^3 cm^2/V sec, and partly, since μ changes very little below threshold, to the higher thresholds. More significant is the fact that, except for Thim and HKI-1, the fields at which the minimum or valley occurs are all higher than the calculated values. In the cases of Thim and HKI-1 the valley location may have been obscured by the generation of carriers referred to earlier. Also significant is the fact that most of the experimental curves lie above the theoretical curves at the higher fields.

If the experimental determinations were all correct, and the different results due to differences in the samples (other than relatively obvious ones such as macroscopic inhomogeneity), the existence of the different v_d versus E curves would signify different heating of the carriers in different samples for a given field. One source of such differences is the formation, discussed earlier, of space-charge regions due to compensation. This operates to cool the distribution in two ways. First, by causing a nonuniform voltage distribution in the sample, with the higher voltage across the space-charge regions which are depleted of carriers, it reduces the field experienced by the carriers below the average field. Second, the reduction in mean free path of the light electrons, described quantitatively by the introduction of τ_s, also results in cooling, as seen earlier. There is some evidence that space-charge scattering is playing a role in the experimental results. The thresholds observed in semi-insulating material, in which space-charge scattering should not play an important role, are lower than those generally observed for samples with $10^{14}\leq n\leq10^{16}$/cm^3. There is also evidence[64] for a low Gunn threshold in samples with very low ρ, 0.01 Ω cm, where again the effects of space-charge scattering should be small.

Another type of effect that would cool the carrier distributions, particularly in semi-insulating and high ρ semiconducting samples, is preferential trapping of high-energy carriers. It has already been indicated that the trapping time decreased with increasing energy in Chang and Moll's sample. In the data shown by Ruch and Kino,[54] for a field of 1.2 kV/cm the trapping time $\tau_{tr}\simeq15$ nsec, while at 5.75 kV/cm, well past the maximum in v_d, τ_{tr} is clearly smaller since the same decrease in current occurs in about half the time. It must be

[58] D. M. Chang and J. L. Moll, Appl. Phys. Letters **9**, 238 (1966).
[59] J. G. Ruch and J. L. Moll, Stanford University (private communication).
[60] A. L. McWhorter and A. G. Foyt, Appl. Phys. Letters **9**, 300 (1966).
[61] J. A. Copeland, Phys. Letters **24A**, 9 (1967).
[62] B. J. Elliott, IBM Laboratories (private communication).
[63] C. Hamaguchi, University of Osaka (private communication).
[64] K. K. N. Chang, S. G. Liu, and H. J. Prager, Appl. Phys. Letters **8**, 196 (1966).

pointed out, however, that τ_{tr}'s very much smaller than 10 nsec would be required to affect the shape of the distribution. Since electron-electron collisions are unimportant, the shape is clearly independent of the number of carriers and would only be affected by a τ_{tr} of the order of the relaxation time, i.e., $\sim 10^{-12}$ sec for high-energy light electrons. Thus τ_{tr} for high-energy electrons would have to be much smaller than τ_{tr} for thermal electrons, by a factor of 10^4 for the Ruch and Kino sample, more like 10^2 for the usual semi-insulating sample. Such a factor is not implausible. For example, calculations show that the probability of tunneling through the Coulomb barrier[65] of a triply charged repulsive center in GaAs increases by a factor of 3×10^3 as the electron energy ε goes from the thermal average 0.025 eV to 0.58 eV. This factor is expected to predominate in the cross section Q, although the actual ε dependence of Q will depend also on the (unknown) mechanism by which the carrier gives up its energy. Since $\tau_{tr} \propto 1/Qv$, the ε dependence stemming from Q will be enhanced by the factor $1/v$. Still steeper ε dependence of Q and τ_{tr} might be obtained due to capture at charged disolcation lines.[65]

Any source of inelastic scattering would also result in a depletion of high-energy light electrons. A clear source of such scattering in semi-insulating GaAs is ionization and excitation of electrons bound to impurities. There is a suggestion of such ionization in the data of Ruch and Kino. At 3.3 kV/cm there is no change in current, or perhaps a slight increase, during the transit time of the carriers, but there is a long tail at the end of the pulse, presumably due to trapped carriers. At 5.75 kV/cm apparently trapping predominates over generation.

A decrease in the population of high-energy light electrons, due to whatever cause, will necessarily result in a decrease in the heavy-electron population. We can estimate this as follows. In a steady state the rate of transition from the central to the upper valleys must balance the reverse rate. Since only light electrons with $\varepsilon > 0.36$ eV can make the transition (we neglect the phonon energy, which is small), the steady-state condition is

$$n_2/\langle\tau_{2\to 1}\rangle = n_1(\varepsilon > 0.36)/\langle\tau_{1\to 2}\rangle. \quad (8.2)$$

The ratio of the average transition times $\langle\tau_{2\to 1}\rangle/\langle\tau_{1\to 2}\rangle$ is the product of the ratio of density-of-states masses, 70:1, and a factor depending on the average energy which is somewhat less than unity. For a field of 6 kV/cm, for example, our calculations for $D_{12}=5\times 10^8$ eV/cm give a ratio $n_2/n_1(\varepsilon > 0.36$ eV) of 44:1. This ratio was found to be relatively independent of field, differing from 44:1 by less than 10% in the range 3 to 9 kV/cm. Thus a small decrease in the number of light electrons with $\varepsilon > 0.36$ eV is expected to lead to a decrease about 40 times as large in the number of heavy electrons.

[65] V. L. Bonch-Bruevich, Fiz. Tverd. Tela **6**, 2047 (1964) [English transl.: Soviet Phys.—Solid State **6**, 1615 (1965)].

To illustrate that the effect of this on v_d may be quite large, we shall again use some of the results obtained for $D_{12}=5\times 10^8$ eV/cm. According to these, at a field of 6 kV/cm, 12% of the electrons are in valley 1, one-sixth of these having $\varepsilon > 0.36$ eV, and the remaining 88% are in valley 2. Because of their lower mobility, the electrons in valley 2 contribute only 20% of the current, while 80% is due to the light electrons, 54% to those with $\varepsilon < 0.36$ eV, and 26% to those with $\varepsilon > 0.36$ eV. To simplify our estimate we shall assume that trapping results in a cooler distribution characterized by only half as many light electrons with $\varepsilon > 0.36$ eV, while the number of light electrons with $\varepsilon < 0.36$ eV is unaffected. Reduction of the former group by $\frac{1}{2}$ will, as discussed earlier, cause a reduction of the heavy electrons by the same factor. The proportion of light electrons in the distribution has thus increased from 12 to 20%, with a corresponding decrease in the percentage of heavy electrons. The ratio of the drift velocity for the cooler distribution to that for the normal distribution is given by

$$v_d'/v_d = \{[n_1'/(n_1'+n_2')]v_1 + [n_2'/(n_1'+n_2')]v_2\}/ \{[n_1/(n_1+n_2)]v_1 + [n_2/(n_1+n_2)]v_2\}, \quad (8.3)$$

where the primes denote quantities relating to the cooler distribution and v_i is the drift velocity of carriers of type i. With the numbers given above for relative current contributions and numbers of carriers, we obtain $v_1/v_2 = 30$. This and the other numbers given above lead to $v_d'/v_d = 1.5$. It is clear that such cooling of the distribution can considerably increase the measured drift velocity.

The conclusion to be reached from the above discussion is that defects may play a profound role in modifying the high-field distribution function in GaAs samples, and therefore the properties dependent on it, such as drift velocity and multiplication rate α. The latter, determined by the high-energy tail of the distribution, would be particularly sensitive to effects of the type we have been discussing. A decision as to whether, in fact, defects are playing such a role awaits further clarification of the differences found experimentally and the availability of material with fewer defects.

ACKNOWLEDGMENTS

We are grateful to S. Barton for assistance in programming and L. Ellicott for running the computer. D. Baird contributed materially to our ideas on the effects of trapping. One of us (E.M.C.) wishes to acknowledge the hospitality of the Division of Applied Physics and the Microwave Laboratory of Stanford University during the final stages of this work.

APPENDIX: COLLISION OPERATORS FOR NONPARABOLIC BANDS

None of the interactions dealt with here are strong, and the required collision operators may be obtained by

the use of ordinary time-dependent perturbation theory. With this the collision operator may be written

$$\left[\frac{\partial f(\mathbf{k})}{\partial t}\right]_c=\frac{2\pi}{\hbar}\sum_{\mathbf{k}'}\left[|(N_q+1|H'|N_q)|^2\delta(\varepsilon-\varepsilon'+\hbar\omega)f(\mathbf{k}')\right.$$
$$+|(N_q-1|H'|N_q)|^2\delta(\varepsilon-\varepsilon'-\hbar\omega)f(\mathbf{k}')$$
$$-|(N_q+1|H'|N_q)|^2\delta(\varepsilon'-\varepsilon+\hbar\omega)f(\mathbf{k})$$
$$\left.-|(N_q-1|H'|N_q)|^2\delta(\varepsilon'-\varepsilon-\hbar\omega)f(\mathbf{k})\right], \quad \text{(A1)}$$

where H' represents the perturbing potential, ε and ε' the energies of states with wave vector $\mathbf{k}$ and $\mathbf{k}'$, respectively. The first two terms of (A1) correspond to scattering from $\mathbf{k}'$ into $\mathbf{k}$ by emission and absorption, respectively, and for these the summation over $\mathbf{k}'$ is to be taken over all possible initial states. The last two terms correspond to scattering out of $\mathbf{k}$ into $\mathbf{k}'$ by emission and absorption, respectively, and here the summation is to be taken over all possible final states.

For polar scattering the absolute square of the matrix element between states $\mathbf{k}'$ and $\mathbf{k}$ is[14]

$$|(\mathbf{k}'|H_{po}'|\mathbf{k})|^2=\frac{2\pi\hbar^2eE_0}{Vm_1|\mathbf{k}'-\mathbf{k}|^2}\begin{Bmatrix}N_q+1\\N_q\end{Bmatrix}, \quad \text{(A2)}$$

where E_0 is defined in (3.2), V is the volume of the crystal, and the upper factor in braces is to be used for emission, the lower for absorption. Note that the matrix element is not dependent on mass because E_0 is proportional to m_1. There is, however, as discussed in Sec. 3, an additional dependence on $\mathbf{k}$ not shown here, which takes the form of a factor that is unity at the bottom of the band and decreases somewhat as $\mathbf{k}$ increases due to the admixture of p-type wave functions.[14] This factor is omitted in the present calculations.

Inserting the matrix element (A2), converting the summation to an integration, and making use of the fact that the δ function is an even function of its argument, we obtain

$$\left(\frac{\partial f}{\partial t}\right)_{po}=\frac{heE_0}{2\pi m_1}\int_{k'=0}^{\infty}\int_{\theta'=0}^{\pi}\int_{\varphi'=0}^{2\pi}\{\delta(\varepsilon'-\varepsilon-\hbar\omega_l)[(N_{ql}+1)f(\mathbf{k}')-N_{ql}f(\mathbf{k})]+\delta(\varepsilon'-\varepsilon+\hbar\omega_l)$$
$$\times[N_{ql}f(\mathbf{k}')-(N_{ql}+1)f(\mathbf{k})]\}\frac{k'^2}{|\mathbf{k}'-\mathbf{k}|^2}\sin\theta'd\theta'd\varphi'dk'. \quad \text{(A3)}$$

The quantity $1/|\mathbf{k}'-\mathbf{k}|^2$ may be expanded as a series of Legendre polynomials in $\cos\alpha$, where α is the angle between $\mathbf{k}$ and $\mathbf{k}'$, e.g.,

$$\frac{1}{|\mathbf{k}'-\mathbf{k}|^2}=\frac{1}{2k'k}\sum_{n=0}^{\infty}(2n+1)Q_n\left(\frac{k'^2+k^2}{2k'k}\right)P_n(\cos\alpha), \quad \text{(A4)}$$

the Q_n being Legendre functions of the second kind.[66] It will be convenient to take the z axis in the direction of $\mathbf{E}$. Then, by the addition theorem,

$$P_n(\cos\alpha)=P_n(\cos\theta)P_n(\cos\theta')+2\sum_{m=1}^{n}\frac{(n-m)!}{(n+m)!}P_n^m(\cos\theta)P_n^m(\cos\theta')\cos m(\varphi-\varphi'). \quad \text{(A5)}$$

The only dependence on θ' and φ' in the integrand of (A3), apart from $1/|\mathbf{k}'-\mathbf{k}|^2$, is in $f(\mathbf{k}')$ which, as discussed in Sec. 5, takes for the lower valley the form $f_1(\varepsilon')+k'\cos\theta'g_1(\varepsilon')$. The θ' and φ' integrations are then readily carried out, with the result

$$\left(\frac{\partial f^{(1)}}{\partial t}\right)_{po}=\frac{heE_0}{m_1k}\int_0^{\infty}(\delta(\varepsilon'-\varepsilon-\hbar\omega_l)\{(N_{ql}+1)[Q_0f_1(\varepsilon')+k'Q_1\cos\theta g_1(\varepsilon')]-N_{ql}Q_0f^{(1)}(\varepsilon)\}+\delta(\varepsilon'-\varepsilon+\hbar\omega_l)$$
$$\times\{N_{ql}[Q_0f_1(\varepsilon')+k'Q_1\cos\theta g_1(\varepsilon')]-(N_{ql}+1)Q_0f^{(1)}(\varepsilon)\})k'dk', \quad \text{(A6)}$$

where, as earlier, $f^{(1)}(\varepsilon)$ denotes $f_1(\varepsilon)+k\cos\theta g_1(\varepsilon)$. The arguments of Q_0 and Q_1 have been omitted in (A6) for the sake of brevity. When the integration variable is changed from k' to ε' with the use of Eq. (2.4) and integration over ε' is carried out, we obtain

$$\left(\frac{\partial f^{(1)}}{\partial t}\right)_{po}=\frac{eE_0}{\hbar k}\left[\left((N_{ql}+1)\left\{Q_0f_1(\varepsilon')+\frac{[2m_1\gamma(\varepsilon')]^{1/2}}{\hbar}Q_1\cos\theta g_1(\varepsilon')\right\}-N_{ql}Q_0f^{(1)}(\varepsilon)\right)\left(\frac{d\gamma}{d\varepsilon'}\right)\Bigg|_{\varepsilon'=\varepsilon+\hbar\omega_l}\right.$$
$$\left.+\left(N_{ql}\left\{Q_0f_1(\varepsilon')+\frac{[2m_1\gamma(\varepsilon')]^{1/2}}{\hbar}Q_1\cos\theta g_1(\varepsilon')\right\}-(N_{ql}+1)Q_0f^{(1)}(\varepsilon)\right)\left(\frac{d\gamma}{d\varepsilon'}\right)\Bigg|_{\varepsilon'=\varepsilon-\hbar\omega_l}\right], \quad \text{(A7)}$$

[66] See, for example, P. M. Morse and H. Feshbach, *Methods of Theoretical Physics* (McGraw-Hill Book Co., New York, 1953), p. 752.

where, in terms of ε',

$$Q_0\left(\frac{k'^2+k^2}{2k'k}\right)=\ln\left\{\frac{\gamma^{1/2}(\varepsilon')+\gamma^{1/2}(\varepsilon)}{|\gamma^{1/2}(\varepsilon')-\gamma^{1/2}(\varepsilon)|}\right\}, \tag{A8a}$$

$$Q_1\left(\frac{k'^2+k^2}{2k'k}\right)=\frac{\gamma(\varepsilon')+\gamma(\varepsilon)}{2\gamma^{1/2}(\varepsilon')\gamma^{1/2}(\varepsilon)}\ln\left[\frac{\gamma^{1/2}(\varepsilon')+\gamma^{1/2}(\varepsilon)}{|\gamma^{1/2}(\varepsilon')-\gamma^{1/2}(\varepsilon)|}\right]-1. \tag{A8b}$$

Separating out the terms in f_1, we obtain

$$\left(\frac{\partial f_1}{\partial t}\right)_{p0}=\frac{eE_0}{(2m_1\gamma(\varepsilon))^{1/2}}\frac{1}{e^{x_l}-1}\Big[\{e^{x_l}f_1(\varepsilon+\hbar\omega_l)-f_1(\varepsilon)\}\Omega_1(\varepsilon+\hbar\omega_l)\left(\frac{d\gamma}{d\varepsilon}\right)\Big|_{\varepsilon+\hbar\omega_l}$$
$$+\{f_1(\varepsilon-\hbar\omega_l)-e^{x_l}f_1(\varepsilon)\}\Omega_1(\varepsilon)\left(\frac{d\gamma}{d\varepsilon}\right)\Big|_{\varepsilon-\hbar\omega_l}\Big], \tag{A9}$$

where $\Omega_1(\varepsilon)$ is defined in Eq. (3.4). From the remaining terms we obtain

$$\left(\frac{\partial k_E g_1(\varepsilon)}{\partial t}\right)_{po}=\frac{eE_0\cos\theta}{\hbar(e^{x_l}-1)}\Big\{e^{x_l}g_1(\varepsilon+\hbar\omega_l)\left[\frac{\gamma(\varepsilon+\hbar\omega_l)}{\gamma(\varepsilon)}\right]^{1/2}\left[\frac{\gamma(\varepsilon+\hbar\omega_l)+\gamma(\varepsilon)}{2\gamma^{1/2}(\varepsilon+\hbar\omega_l)\gamma^{1/2}(\varepsilon)}\Omega_1(\varepsilon+\hbar\omega_l)-1\right]\left(\frac{d\gamma}{d\varepsilon}\right)\Big|_{\varepsilon+\hbar\omega_l}$$
$$+g_1(\varepsilon-\hbar\omega_l)\left[\frac{\gamma(\varepsilon-\hbar\omega_l)}{\gamma(\varepsilon)}\right]^{1/2}\left[\frac{\gamma(\varepsilon-\hbar\omega_l)+\gamma(\varepsilon)}{2\gamma^{1/2}(\varepsilon-\hbar\omega_l)\gamma^{1/2}(\varepsilon)}\Omega_1(\varepsilon)-1\right]\left(\frac{d\gamma}{d\varepsilon}\right)\Big|_{\varepsilon-\hbar\omega_l}$$
$$-g_1(\varepsilon)\Omega_1(\varepsilon+\hbar\omega_l)\left(\frac{d\gamma}{d\varepsilon}\right)\Big|_{\varepsilon+\hbar\omega_l}-e^{x_l}g_1(\varepsilon)\Omega_1(\varepsilon)\left(\frac{d\gamma}{d\varepsilon}\right)\Big|_{\varepsilon-\hbar\omega_l}\Big\}. \tag{A10}$$

For a parabolic band, where $\gamma(\varepsilon)=\varepsilon$ and $d\gamma/d\varepsilon=1$, (A9) and (A10) are easily shown to be identical with the expressions derived by Howarth and Sondheimer[13] for that case.

It is useful to have expressions for (A9) and (A10) for the limit $\varepsilon\gg\hbar\omega_l$. Expanding $f_1(\varepsilon\pm\hbar\omega_l)$ and $\gamma(\varepsilon\pm\hbar\omega_l)$ to terms of order $(\hbar\omega_l/\varepsilon)^2$, and writing the results in terms of $x=\varepsilon/\hbar\omega_l$ and $\Gamma(x)\equiv\gamma(\varepsilon)/\hbar\omega_l$, we obtain from (A.9)

$$\left(\frac{\partial f_1}{\partial t}\right)_{po}\underset{x\gg1}{\rightarrow}\frac{eE_0}{(2m_1\hbar\omega_l\Gamma)^{1/2}}\Big\{\frac{1}{2}\frac{e^{x_l}+1}{e^{x_l}-1}\Gamma'\ln\left(\frac{4\Gamma}{\Gamma'}\right)f_1''$$
$$+\left[\Gamma'\ln\left(\frac{4\Gamma}{\Gamma'}\right)+\frac{e^{x_l}+1}{e^{x_l}-1}\Gamma''\ln\left(\frac{4\Gamma}{\Gamma'}\right)+\frac{1}{2}\frac{e^{x_l}+1}{e^{x_l}-1}\left(\frac{\Gamma'}{\Gamma}-\frac{\Gamma''}{\Gamma'}\right)\Gamma'\right]f_1'+\left[2\Gamma''\ln\left(\frac{4\Gamma}{\Gamma'}\right)+\left(\frac{\Gamma'}{\Gamma}-\frac{\Gamma''}{\Gamma'}\right)\Gamma'\right]f_1\Big\}, \tag{A11}$$

where a prime indicates d/dx. From (A10) to lowest order in $\hbar\omega_l/\varepsilon$ we obtain

$$\left(\frac{\partial k_E g_1}{\partial t}\right)_{po}\underset{x\gg1}{\rightarrow}-k_E g_1\left[\frac{eE_0}{(2m_1\hbar\omega_l)^{1/2}}\frac{e^{x_l}+1}{e^{x_l}-1}\frac{\Gamma'}{\Gamma^{1/2}}\right]. \tag{A12}$$

In this limit therefore a relaxation time exists for the polar mode scattering given by

$$\tau_{po}=\frac{(2m_1\hbar\omega_l)^{1/2}}{eE_0}\frac{e^{x_l}-1}{e^{x_l}+1}\frac{\Gamma^{1/2}}{\Gamma'}. \tag{A13}$$

Expressions similar to (A11)–(A13) have been obtained for the high-temperature limit, i.e., $T\gg\Theta$, by Kolodziejczak,[21] and Dykman and Tomchuk.[18]

To obtain the collision operator for intervalley scattering when one or both of the valleys is nonparabolic we may again start from (A1). For scattering from a state with wave vector $\mathbf{k}^{(i)}$ in valley i to $\mathbf{k}^{(j)}$ by absorption or emission of a phonon, the absolute square of the matrix element[67] is

$$|(\mathbf{k}^{(j)},N_q\pm1|H_{ij}'|\mathbf{k}^{(i)},N_q)|^2=\frac{D_{ij}^2\hbar}{2V\rho\omega_{ij}}\begin{Bmatrix}N_q+1\\N_q\end{Bmatrix}, \tag{A14}$$

where

$$\mathbf{k}^{(j)}=\mathbf{k}^{(i)}\pm\mathbf{q} \tag{A15}$$

and D_{ij} is the coupling constant, ω_{ij} the angular frequency of the phonon connecting valleys i and j. N_q here is, of course, the number of phonons with angular frequency ω_{ij}. It is advantageous in this case to consider separately from the beginning the contributions of the spherically symmetric term $f_i(\varepsilon)$ and the drift term $k_E g_i(\varepsilon)$. We shall calculate first $(\partial f_i(\mathbf{k})/\partial t)_{i\rightleftarrows j}$, the rate of change of $f_i(\mathbf{k})$ due to transitions between the ith

[67] C. Herring, Bell System Tech. J. 34, 237 (1955).

and jth valleys. The first two terms of (A1) for this case correspond to electrons scattered from $\mathbf{k}'$ in j into $\mathbf{k}$ in i, while the second two correspond to electrons scattered from $\mathbf{k}$ in i into $\mathbf{k}'$ in j. Since the matrix element is independent of $\mathbf{k}'$ and the argument of the δ function and $f_i(\mathbf{k}')$ depend on $\mathbf{k}'$ only through ε', the summation over $\mathbf{k}'$ may be replaced by a summation or integration over ε'. Thus, for the first two terms of (A1),

$$\sum_{\mathbf{k}'} f_j(\mathbf{k}')\delta(\varepsilon-\varepsilon'\pm\hbar\omega_{ij}) = \int f_j(\varepsilon')\delta(\varepsilon-\varepsilon'\pm\hbar\omega_{ij})\rho_j(\varepsilon')d\varepsilon' = f_j(\varepsilon\pm\hbar\omega_{ij})\rho_j(\varepsilon\pm\hbar\omega_{ij}), \quad \text{(A16)}$$

where $\rho_j(\varepsilon)$ is the number of states per unit energy range in the jth valley. By similar arguments the last two terms of (A1) give, for this case,

$$\sum_{\mathbf{k}'} f_i(\mathbf{k})\delta(\varepsilon'-\varepsilon\pm\hbar\omega_{ij}) = f_i(\varepsilon)\int \delta(\varepsilon'-\varepsilon\pm\hbar\omega_{ij})\rho_j(\varepsilon')d\varepsilon' = f_i(\varepsilon)\rho_j(\varepsilon\mp\hbar\omega_{ij}). \quad \text{(A17)}$$

Thus from (A1) with the use of (A14)–(A17) we obtain

$$\left(\frac{\partial f_i(k)}{\partial t}\right)_{i\rightleftarrows j} = \frac{\pi D_{ij}^2}{V\rho\omega_{ij}}[(N_q+1)f_j(\varepsilon+\hbar\omega_{ij})\rho_j(\varepsilon+\hbar\omega_{ij}) + N_q f_j(\varepsilon-\hbar\omega_{ij})\rho_j(\varepsilon-\hbar\omega_{ij}) - (N_q+1)f_i(\varepsilon)\rho_j(\varepsilon-\hbar\omega_{ij}) - N_q f_i(\varepsilon)\rho_j(\varepsilon+\hbar\omega_{ij})]. \quad \text{(A18)}$$

It is clear from (A18) that nonparabolicity of the ith valley does not affect its collision operator, which depends only on the density of states in the jth valley. So far as intervalley scattering is concerned, the only modification required due to nonparabolicity will be in the contribution to the collision operator for the $\langle 100\rangle$ valleys of scattering to the (0,0,0) valley. Denoting the (0,0,0) valley by index 1 and the set of $\langle 100\rangle$ valleys by index 2, we have for the respective densities-of-states of either spin

$$\rho_1(\varepsilon) = \frac{m_1^{3/2}V\gamma^{1/2}(\varepsilon)}{2^{1/2}\pi^2\hbar^3}\frac{d\gamma}{d\varepsilon} \quad \text{(A19a)}$$

and

$$\rho_2(\varepsilon) = (m_2^{(N)})^{3/2}V(\varepsilon-\varepsilon_{02})^{1/2}/2^{1/2}\pi^2\hbar^3, \quad \text{(A19b)}$$

where ε_{02} is the minimum of the upper valleys. Inserting (A19a) into (A18) and expressing N_q in terms of $x_{12}\equiv\hbar\omega_{12}/k_0T$, we obtain for the collision operator of the $\langle 100\rangle$ valley distribution due to intervalley scattering involving the (0,0,0) valley

$$\left(\frac{\partial f_2}{\partial t}\right)_{2\rightleftarrows 1} = \left(\frac{m_1}{m_2^{(N)}}\right)^{3/2}\frac{1}{\tau_{12}\varepsilon_{02}^{1/2}}\{\gamma^{1/2}(\varepsilon+\hbar\omega_{12})\gamma'(\varepsilon+\hbar\omega_{12}) \times[e^{x_{12}}f_1(\varepsilon+\hbar\omega_{12})-f_2(\varepsilon)]+\gamma^{1/2}(\varepsilon-\hbar\omega_{12})\gamma'(\varepsilon-\hbar\omega_{12}) \times[f_1(\varepsilon-\hbar\omega_{12})-e^{x_{12}}f_2(\varepsilon)]\}, \quad \text{(A20)}$$

where

$$\frac{1}{\tau_{12}} = \frac{D_{12}^2[m_2^{(N)}]^{3/2}\varepsilon_{02}^{1/2}}{2^{1/2}\pi\hbar^3\rho\omega_{12}}\frac{1}{e^{x_{12}}-1}. \quad \text{(A21)}$$

It can be shown by the principle of detailed balancing that $D_{21}=D_{12}$.

For the rate of change of f_1 due to intervalley scattering involving the $\langle 100\rangle$ valleys, we obtain after summation of (A18) over the equivalent $\langle 100\rangle$ valleys

$$\left(\frac{\partial f_1}{\partial t}\right)_{1\rightleftarrows 2} = \frac{1}{\tau_{12}\varepsilon_0^{1/2}}\{(\varepsilon+\hbar\omega_{12}-\varepsilon_{02})^{1/2} \times[e^{x_{12}}f_2(\varepsilon+\hbar\omega_{12})-f_1(\varepsilon)]+(\varepsilon-\hbar\omega_{12}-\varepsilon_{02})^{1/2} \times[f_2(\varepsilon-\hbar\omega_{12})-e^{x_{12}}f_1(\varepsilon)]\}. \quad \text{(A22)}$$

We consider now the remainder of the intervalley scattering collision operator, $(\partial k_E g_i/\partial t)_{i\rightleftarrows j}$. It is readily seen that the first two terms of (A1) make no contribution because $k_E'\equiv k'\cos\theta'$, and this causes the integral to vanish when integration over θ' is carried out. This is, of course, expected because a relaxation time is known to exist for intervalley scattering. The summations required for the second pair of terms of (A1) are again given by (A17), and we may write down directly

$$\left(\frac{\partial k_E g_i}{\partial t}\right)_{i\to j} \equiv -\frac{k_E g_i}{\tau_{i\to j}^{(i)}} = -k_E g_i\left\{\frac{\pi D_{ij}^2}{V\rho\omega_{ij}}[(N_q+1) \times\rho_j(\varepsilon-\hbar\omega_{ij})+N_q\rho_j(\varepsilon+\hbar\omega_{ij}]\right\}. \quad \text{(A23)}$$

It is to be remembered throughout that terms of the form $(\varepsilon\pm\hbar\omega-\varepsilon_{02})^{1/2}$ or $\gamma^{1/2}(\varepsilon\pm\hbar\omega)$ are to be included only if the argument of the square root is positive. This is required in order that energy be conserved in the process concerned.